Modelling and optimizing testing strategies for epidemic outbreaks

Ph.D. Thesis

Tamás Tekeli

Supervisor:

Gergely Röst, associate professor, Ph.D.

Doctoral School of Mathematics
and Computer Science
University of Szeged, Bolyai Institute

Szeged

2022

Acknowledgements

Firstly, I would like to express my sincere gratitude to my supervisor Gergely Röst for the continuous support of my Ph.D. study and related research, for his patience, motivation and immense knowledge. His guidance helped me in all the time of research and writing of this thesis.

I am also thankful to Attila Dénes, whom we have been working for four years with. He motivated me greatly and taught me a lot about dynamical systems and mathematical modelling.

I am also grateful for the support of the Doctoral School in Mathematics and Computer Science, to the Bolyai Institute as a whole and to my colleagues in the National Laboratory of Health Security.

I would like to thank my parents and my brother for their continued support that started from my childhood and has been continuing until this moment.

Last but not least, I am very thankful to my extended family and my friends.

My special thanks go to all my current and former teammates at Újszegedi Torna Club for their moral guidance and support throughout the writing of this thesis.

Contents

1

Introduction

The aim of the thesis is to develop and analyse dynamical models for the transmission dynamics and propagation of infectious diseases. Our approach can be used to the practical problems of epidemiology, with serious implications to public health policy, prevention, control and mitigation strategies in public health emergencies such as the ongoing pandemic.

Mathematical epidemiology is a rapidly developing area of mathematical applications in life sciences. Infectious disease modelling complements traditional epidemiological tools and contributes to the synergistic approach to complex public health problems. Mathematical methods are extremely important also to devise adaptive strategies for various epidemiological situations.

Diseases have always been an important part of the life of societies. Since the beginning of written history there have been records of epidemics causing significant burden on human populations, often recurring years or decades later. For example, the Black Death spread from Asia throughout Europe in waves beginning in 1346, and is estimated to have caused the death of more than 30% of the population of Europe between 1346 and 1350. The disease returned regularly in several parts of Europe for centuries, most famously as the Great Plague of London in 1665-1666. After the first World War, the Spanish flu estimated to cause 25 - 50 million deaths worldwide, followed by other severe influenza pandemics in the 50's and 60's. There are still annual influenza epidemics that cause up to 650,000 fatalities worldwide, according to WHO. Recently, we are struggling with the COVID-19 pandemic, with 6,400,000 reported deaths until September 2022, while the true number of deaths may reach 20 millions.

There are also potentially fatal diseases that have become endemic in some populations. Every year, millions of people die of avoidable diseases such as measles, respiratory infections, diarrhea, and other, always-present diseases. Diseases such as malaria, typhus, cholera are endemic in many parts of the world. The impact of high disease mortality and morbidity in these countries are significant. The World Health Organization has estimated that in 2020 there were 1,500,000 deaths due to tuberculosis, 650,000 fatalities due to HIV/AIDS, and 627,000 due to malaria. In 1980 there were 2,600,000 deaths due to measles, but the widespread vaccination campaigns resulted in a 73% drop in fatalities between 2000 and 2018 worldwide.

The objective of medical screening and testing is to identify the disease in its still curable phase. This may have been an old challenge in medicine and for a successful testing at least

four conditions need to be met: the availability of simple, validated and acceptable forms of tests, the discovery of effective treatments, the establishment of a screening protocol, and the wide access to health care. There are many successes from the history of medical screening: testing for syphilis in the United States army (one of the first applications of group testing), screening for cervical cancer using the Pap test, and screening for breast cancer by mammography. The evaluation of the impact of screening on human health slowly progressed, from obvious changes in the vital statistics to less obvious such as the decline in mortality of cancer of the uterus, to finally more subtle changes, such as the impact of mammography screening on breast cancer mortality.

Screening in non-infectious diseases such as cancer has the main goal of early identification of cases that drastically increases the chance of successful treatment for that individual. The main advantage of testing in combating infectious diseases beyond treating the tested individual is that it enables to recognize asymptomatic infected, who may have a very important role in disease transmission dynamics, thus potentially by breaking chains of infection the testing benefits indirectly all other member of the population. Hence, strategic testing can be used as a mitigation tool of the epidemic on the population level. Testing helps to estimate the proportion of asymptomatic carriers and their role in disease spread. It also helps to find clusters of cases and to have a more precise estimate on transmission rates and death rates. With the application of these results, testing provides a guide to make decisions on social distancing policy and other measures including the allocation of medical resources.

In Chapter 2, we present an overview for one of the simplest SIS epidemiological model, then we discuss some of the most important and feasible extensions and generalizations. Then, we introduce a basic mass-testing and isolation intervention and we point out that this simple alteration induces a completely different and richer dynamics.

In Chapters 3 and 4, we investigate the mathematical analysis of multistage SIS models. We calculate the basic reproduction number $\mathcal{R}_0$, and discuss the existence of the endemic equilibrium. Our main result is that the stability of the endemic equilibrium depends strongly on the number of stages: the endemic equilibrium is always stable when $n \leq 3$, while for any $n > 3$ it can be either stable or unstable, depending on the particular choice of the parameters. We generalize previous stability results for $SIRS$ models as well and point out a mistake in the literature for multistage $SEIRS$ models.

In Chapter 5, we consider an extended $SEIR$-type model for the transmission dynamics of COVID-19. We incorporate symptom-based testing of patients and isolation upon positive result *i.e.* removal from the chain of transmission. The clinical symptoms that trigger the testing of individuals is referred to as *indicator symptoms*. The *force of testing* is defined as the per capita rate at which infected individuals are tested. It is described by a nonlinear function of the state of the epidemic and of all individuals displaying the indicator symptom at a given time, with or without COVID-19 infection, hence, it is considerably different from previous approaches. Our goal is to understand the impact, and especially the limitations of this testing strategy, hence we model neither contact-tracing of patients with positive tests nor the testing of a fraction of non-symptomatic contacts, both of which are common and efficient improvements and result in removal of additional patients from the chain of transmission.

In Chapter 6, we develop a compartmental model to study the applicability of group

testing and compare different pooling strategies: regular and Dorfman pooling. The model includes isolated compartments as well, from where individuals rejoin the active population after some time delay. We develop a method to optimize Dorfman pooling depending on disease prevalence and establish an adaptive strategy to select variable pool sizes during the course of the epidemic. It is shown that optimizing the pool size can avert a significant number of infections. The adaptive strategy is much more efficient, and may prevent an epidemic outbreak even in situations when a fixed pool size strategy can not.

2

SIS epidemic models

2.1 Simple dynamics

Compartmental models of infectious diseases are based on a partition of the population according to their disease status [20]. Some diseases, for example, those from some of the upper respiratory and sexually transmitted diseases, do not confer any long-lasting immunity. Upon recovery from infection, individuals can therefore be assumed to be susceptible again. This simple approach results in the SIS model, which considers the proportion of the population that are susceptible to (S), or infected with (I) the particular disease. The simplest SIS model is

$$S'(t) = -\beta S(t)I(t) + \gamma I(t), \tag{2.1}$$
$$I'(t) = \beta S(t)I(t) - \gamma I(t), \tag{2.2}$$

where β is the transmission rate and γ is the recovery rate.

Note that if the total population is normalized to unity, with denoting $S(t) = S$, $I(t) = I$ it holds that:

$$S'(t) + I'(t) = 0, \text{ and } S(t) + I(t) = 1.$$

Therefore,

$$I' = \beta\,(1 - I)\,I - \gamma I = \beta I\left(1 - \frac{\gamma}{\beta} - I\right). \tag{2.3}$$

Thus, the dynamics of the infected population is equivalent to the dynamics of the logistic equation, so that for all $I(0) \geq 0$ it holds that

$$\text{if } \frac{\beta}{\gamma} < 1, \text{ then } \lim_{t\to\infty} I(t) = 0;$$
$$\text{if } \frac{\beta}{\gamma} \geq 1, \text{ then } \lim_{t\to\infty} I(t) = 1 - \frac{\gamma}{\beta}.$$

The expression $\dfrac{\beta}{\gamma}$ shows the expected number of new infections directly generated by one infectious person in a completely susceptible population. This is called the basic reproduction

number, denoted $\mathcal{R}_0$. It is possible to determine the analytical solution to this model. Rewriting the right-hand side of (2.3) as

$$I' + (\gamma - \beta)I = -\beta I^2$$

and assuming $I \not\equiv 0$, $I(0) = I_0$, substituting

$$u = \frac{1}{I},$$
$$u' = -\frac{1}{I^2} \cdot I'$$

transforms (2.3) to the first order linear equation

$$\begin{aligned} -u' + (\gamma - \beta)u &= -\beta, \\ u(0) &= \frac{1}{I_0}. \end{aligned} \tag{2.4}$$

If $\mathcal{R}_0 = \dfrac{\beta}{\gamma} = 1$, then we have the solution as

$$I(t) = \frac{1}{\beta t + \frac{1}{I_0}}.$$

Otherwise, solving (2.4) and substituting back yields

$$I(t) = \frac{\frac{\beta-\gamma}{\beta}}{1 + \left(\frac{\beta-\gamma}{\beta} \cdot \frac{1}{I_0}\right) e^{(\gamma-\beta)t}}.$$

As mentioned, the system is assumed to be closed, so the susceptible population is then $S(t) = 1 - I(t)$.

2.2 Extensions of the SIS model

A major simplification in the SIS model is the exponential distribution of the infectious period, emerging from the assumption that individuals recover with a constant rate. This assumption means that the chance of an individual progressing during any given time period does not depend on the elapsed time since the individual became infected. While such a simplification highly facilitates mathematical analysis, it is not realistic in most situations. Hence, we aim include a more faithful representation of the time distributions of infectious periods in the models.

A reasonable extension to make the simple SIS model more realistic is to divide the infectious period into stages $I_1, I_2, \ldots, I_n$, following the progression of the disease within the host, given that the infectiousness of an individual may change during the course of infection. Epidemic processes of this kind have focused on establishing systems of equations describing the number of individuals at each stage of the epidemic, and the rates of progression from

compartments I_k to I_{k+1}. Epidemic models with stage structure (see for example [23, 26, 27, 29]) and more general SIS models ([21, 28]) have been widely analyzed in the literature.

In the multi-stage framework, it is assumed that the disease progression is characterised by a number of distinct stages, with the duration of each stage being exponentially distributed. Due to the fact that the sum of independent exponentially distributed random variables follows a hypo-exponential distribution, one can replace an exponential distribution with the mean infectious period γ^{-1} by a hypo-exponential distribution that has the same mean infectious period. The so-called *linear chain trick* then consists in replacing a single infectious stage with n exponentially distributed sub-stages as substage I_i having its own mean period γ_i^{-1}. These multiple stages of infection can be used to represent periods of increased or decreased risk of transmitting the disease.

Let's denote the probability of an infected individual whose "infection age" is a by $\mathcal{F}(a)$. This means, that someone is still infected at time t, if he or she got infected at $t-a$. It is straightforward that $\mathcal{F}$ is non-increasing with

$$\mathcal{F} : [0, \infty] \to [0, 1],$$
$$\mathcal{F}(0) = 1 \text{ and } \lim_{t\to\infty} \mathcal{F}(t) = 0.$$

We can extend the previous cases with the help of a probability density function. Let's denote the density of a cohort whose infection age is v at time moment t by $g(t, v)$. Then

$$g(t, v) = \beta \left(1 - I(t - v)\right) I(t - v)\mathcal{F}(v).$$

Integration yields

$$I(t) = \beta \int_0^\infty \left(1 - I(t - v)\right) I(t - v)\mathcal{F}(v)dv. \tag{2.5}$$

Hethcote and van den Driessche made the conjecture that the endemic equilibrium, whenever it exists, is globally asymptomatically stable, regardless of the particular form of $\mathcal{F}$. Röst and Nakata proved in [32] that this conjecture holds, if the support of $\mathcal{F}$ is compact. This approach, though considers constant β infectivity, regardless the infection age. Our assumption was that varying (2.5) to

$$I(t) = \int_0^\infty \beta(v)I(t - v) \left(1 - I(t - v)\right) \mathcal{F}(v)dv \tag{2.6}$$

can cause richer, oscillatory dynamics. In Chapters 3 and 4, we prove this for a discretized version of (2.6) with multiple stages. Moreover, extending (2.1) with introducing a simple testing and isolating method can change its dynamics.

2.3 Oscillations in an SIS system with testing and delay

We consider the following simple delay differential equation model, derived from the basic SIS-setup:

$$\begin{aligned} S'(t) &= -\beta \cdot S(t) \cdot I(t) + \gamma \cdot I(t) + \sigma \cdot I(t - \tau) \\ I'(t) &= \beta \cdot S(t) \cdot I(t) - \gamma \cdot I(t) - \sigma \cdot I(t) \\ Q'(t) &= \sigma \cdot I(t) - \sigma \cdot I(t - \tau). \end{aligned} \tag{2.7}$$

Parameter β stands for the infection rate and γ for the recovery rate. We introduce a testing rate σ for the intervention of testing infected individuals, τ stands for the isolation period. Individuals, who give a positive test spend the isolation time in the quarantine compartment Q. We scaled the population size to $N = S(t) + I(t) + Q(t) = 1$. It's easy to calculate the reproduction number as

$$\mathcal{R}_0 = \frac{\beta}{\gamma + \sigma}.$$

Integrating the equation of Q yields

$$Q(t) = \sigma \int_{t-\tau}^{t} I(s)ds. \tag{2.8}$$

Using (2.8) and the scaling of the population size, we can reduce (2.7) to the scalar equation

$$I'(t) = \beta \cdot I(t) \left(1 - I(t) - \sigma \int_{t-\tau}^{t} I(s)ds\right) - (\gamma + \sigma)\, I(t). \tag{2.9}$$

We can re-scale the delay with temporalily introducing $\tilde{t} = \frac{t}{\tau}$ and $x(\tilde{t}) = I(t)$. Then, $\frac{dx}{d\tilde{t}} = x'(\frac{t}{\tau}) = \tau \cdot I'(t)$ and $I(t-\tau) = I(\tau \cdot \tilde{t} - \tau) = I\left(\tau \cdot \left(\tilde{t} - 1\right)\right) = x\left(\tilde{t} - 1\right)$. Re-scaling the time delay τ also yields

$$\int_{t-\tau}^{t} I(s)ds = \tau \int_{\tilde{t}-1}^{\tilde{t}} x(\tilde{s})d\tilde{s}.$$

Therefore, with interchanging $\tilde{t} \sim t$, we get

$$x'(t) = \tau x(t) \left(\beta - \beta x(t) - \tau\beta\sigma \int_{t-1}^{t} x(s)ds - (\sigma + \gamma)\right). \tag{2.10}$$

To find the equilibria x_∞, we solve the corresponding steady state equation

$$0 = \tau x_\infty \left(\beta - \beta x_\infty - \tau\beta\sigma \int_{t-1}^{t} x_\infty ds - (\sigma + \gamma)\right).$$

Obviously, either $x_{\infty,\mathrm{DFE}} = 0$ (called disease free equilibrium, DFE) , or

$$0 = \beta - \beta x_\infty - \tau\beta\sigma \int_{t-1}^{t} x_\infty ds - (\sigma + \gamma).$$

Thus,

$$0 = \beta - \beta x_\infty - \tau\beta\sigma x_\infty - (\sigma + \gamma),$$

and

$$x_{\infty,\mathrm{EE}} = \frac{\beta - (\sigma + \gamma)}{\beta\,(\tau \cdot \sigma + 1)}. \tag{2.11}$$

It is straightforward that $x_{\infty,\mathrm{EE}}$ (called endemic equilibrium, EE) exists if and only if $R_0 > 1$.

To investigate the local stability of the disease-free equilibrium we have to linearize (2.10) around 0, to obtain the linear part as

$$x'(t) = \tau x(t) \left(\beta - (\gamma + \sigma)\right).$$

Thus, the characteristic equation is given by

$$\lambda = \tau \left(\beta - (\gamma + \sigma)\right).$$

Clearly, with τ being positive, the DFE is unstable if and only if the endemic equilibrium exists.

To address the stability of $x_{\infty,\mathrm{EE}}$, we consider the variational equation around the steady state,

$$x'(t) = \tau \left(x(t) + x_{\infty,\mathrm{EE}}\right) \cdot \left(\beta - \beta \cdot \left(x(t) + x_{\infty,\mathrm{EE}}\right) - \beta\sigma\tau \int_{t-1}^{t} \left(x(s) + x_{\infty,\mathrm{EE}}\right) ds - (\gamma + \sigma)\right).$$

The linear part is

$$\begin{aligned} x'(t) =& x(t) \cdot \left(\beta\tau - 2\beta\tau \cdot x_{\infty,\mathrm{EE}} - \beta\sigma\tau^2 \cdot x_{\infty,\mathrm{EE}} - \tau\left(\gamma + \sigma\right)\right) \\ &+ \left(\beta\tau \cdot x_{\infty,\mathrm{EE}} - \beta\tau \cdot x_{\infty,\mathrm{EE}}^2 - \beta\sigma\tau^2 \cdot x_{\infty,\mathrm{EE}}^2 - \tau\left(\gamma + \sigma\right) \cdot x_{\infty,\mathrm{EE}}\right) \\ &- \beta\sigma\tau^2 \cdot x_{\infty,\mathrm{EE}} \cdot \int_{t-1}^{t} x(s) ds. \end{aligned}$$

Applying the exponential ansatz $x(t) = e^{\lambda t}$ (for $\lambda \neq 0$) gives

$$\begin{aligned} \lambda e^{\lambda t} &= e^{\lambda t} \cdot \left(\beta\tau - 2\beta\tau \cdot x_{\infty,\mathrm{EE}} - \beta\sigma\tau^2 \cdot x_{\infty,\mathrm{EE}} - \tau\left(\gamma + \sigma\right)\right) \\ &\quad + \left(\beta\tau \cdot x_{\infty,\mathrm{EE}} - \beta\tau \cdot x_{\infty,\mathrm{EE}}^2 - \beta\sigma\tau^2 \cdot x_{\infty,\mathrm{EE}}^2 - \tau\left(\gamma + \sigma\right) \cdot x_{\infty,\mathrm{EE}}\right) \\ &\quad - \beta\sigma\tau^2 \cdot x_{\infty,\mathrm{EE}} \cdot \int_{t-1}^{t} e^{\lambda s} ds \\ &= -A \cdot e^{\lambda t} - C \cdot \frac{1}{\lambda} \cdot \left(e^{\lambda t} - e^{\lambda t} \cdot e^{-\lambda}\right), \end{aligned}$$

considering that applying (2.11) yields

$$\left(\beta\tau \cdot x_{\infty,\mathrm{EE}} - \beta\tau \cdot x_{\infty,\mathrm{EE}}^2 - \beta\sigma\tau^2 \cdot x_{\infty,\mathrm{EE}}^2 - \tau\left(\gamma + \sigma\right) \cdot x_{\infty,\mathrm{EE}}\right) = 0.$$

From (2.11) we obtain

$$\begin{aligned} A &= \beta\tau x_{\infty,\mathrm{EE}} \\ C &= \sigma\tau \cdot A. \end{aligned}$$

Rearranging and introducing $k := \sigma\tau$ yields

$$\lambda^2 + A \cdot \lambda - e^{-\lambda} kA + kA = 0. \tag{2.12}$$

We prove that (2.12) can have pure imaginary roots $\lambda = i\omega$ with $\omega > 0$, for suitable A and k. Substituting $z = i\omega$ into (2.12) yields

$$(i\omega)^2 + A \cdot i\omega - e^{-i\omega} kA + kA = 0.$$

The real and imaginary parts of this equation are

(i) $\sin\omega \cdot kA + \omega A = 0$,

(ii) $-\omega^2 + kA - \cos\omega \cdot kA = 0$.

After some rearranging to A and k and considering that $k, \omega > 0$, thus $\sin\omega < 0$ we get

$$k = -\frac{\omega}{\sin\omega}, \tag{2.13}$$

$$A = \frac{\omega \cdot \sin\omega}{\cos\omega - 1}. \tag{2.14}$$

We note that $\sin\omega < 0$ means that $(2n-1)\,\pi \leq \omega \leq 2n\pi$, $n = 1, 2, \ldots$. With elementary calculus we can see that $k = A = \omega = \frac{3\pi}{2}$ serves as a solution.

We also have to check the transversality condition $\mathrm{Re}\left(\frac{\partial\lambda}{\partial k}\right) \neq 0$. In order to obtain this, we differentiate the implicit function

$$F(\lambda(k), k) := \lambda^2 + A \cdot \lambda - e^{-\lambda} \cdot kA + kA = 0$$

to get

$$\frac{\partial\lambda}{\partial k} = \frac{e^{-\lambda}A - A}{2\lambda + A + Ake^{-\lambda}}.$$

Substituting $\lambda = i\omega$, it is enough to show that

$$(\cos\omega \cdot A - A)\,(A + Ak\cos\omega) \neq A\sin\omega\,(2\omega - Ak\sin\omega)\,.$$

Simplifying and expanding yield

$$A\,(\cos\omega - 1)\,(1 + k\cos\omega) \neq 2\omega\sin\omega - Ak\sin^2\omega.$$

Applying (2.14) gives

$$A\,(\cos\omega - 1)\,k\cos\omega \neq \omega\sin\omega - Ak\sin^2\omega,$$

which is equivalent to

$$Ak - Ak\cos\omega \neq \omega\sin\omega,$$

and applying (2.14) again will show that we have to prove that

$$k \neq -1,$$

which obviously holds.

This confirms the possibility of a Hopf-bifurcation, and an unstable parameter setup. Indeed, if we set

$$\beta = \frac{24}{14}, \quad \tau = 14, \quad \gamma = \frac{1}{14}, \quad \sigma = \frac{5}{14} \tag{2.15}$$

the characteristic polynomial will be

$$\lambda^2 + 3 \cdot \lambda + 15 - 15e^{-\lambda}$$

and it will have characteristic roots

$$\lambda \approx 0.0476737 \pm 4.40805i.$$

As a conclusion, we can say that in terms of model dynamics, the simple SIS model is equivalent to the well-known logistic equation, but even a basic extension, such as introducing testing and quarantine of fixed duration can generate much richer dynamics. In the next two chapters, we work with the multistage and discretized version of (2.5).

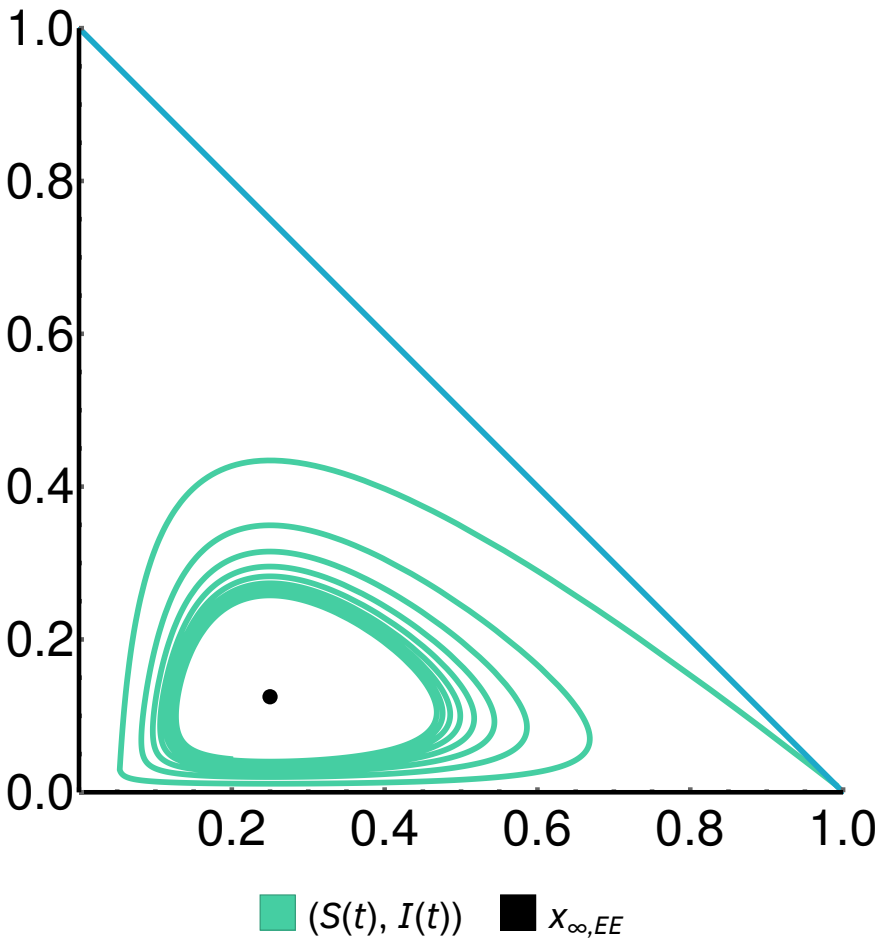

Figure 2.1: SI phase plot of solution paths of (2.7) approaching the periodic solution with parameter configuration (2.15).

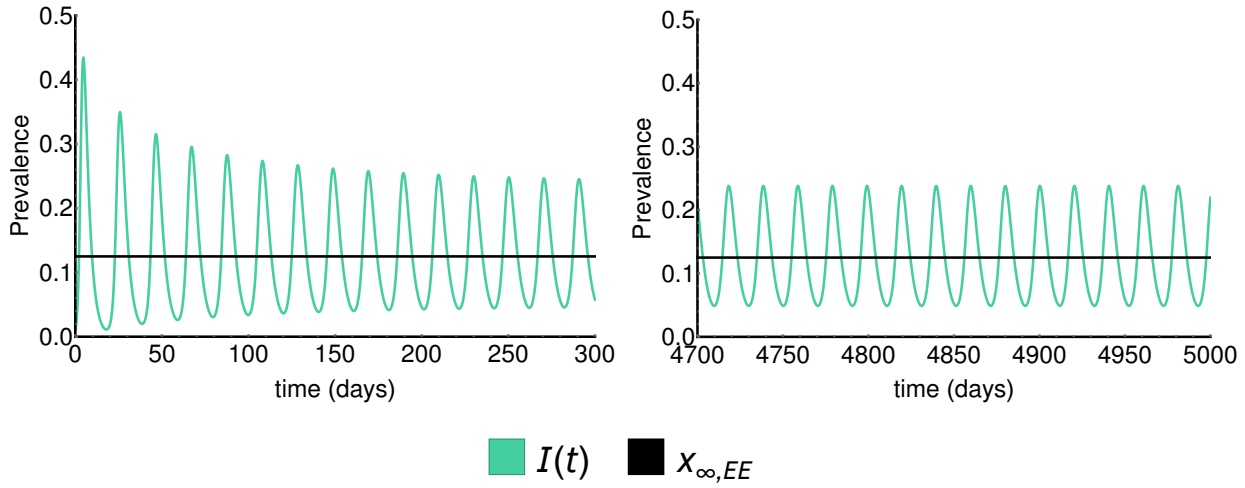

Figure 2.2: Snapshots of an oscillatory solution of system (2.7) with parameter configuration (2.15), with $t \in [0, 300]$ (in the left) and $t \in [4700, 5000]$ (in the right).

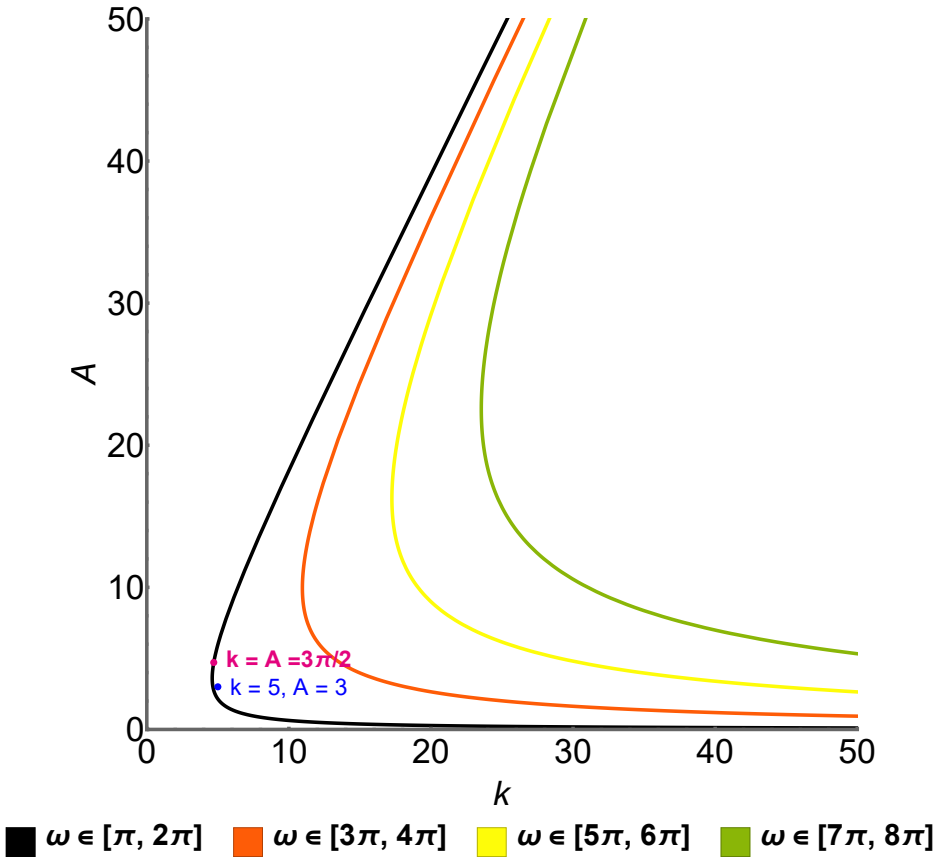

Figure 2.3: Imaginary root curves of (2.12).

3

Stability and instability in multistage SIS models

3.1 Introduction

In this chapter, we consider multistage compartment models of infectious diseases, where infected individuals are passing through infectious stages $I_1, I_2, \dots I_n$ and then return to the susceptible compartment. First we calculate the basic reproduction number $\mathcal{R}_0$, and prove that the disease dies out for $\mathcal{R}_0 \leq 1$, while a unique endemic equilibrium exists for $\mathcal{R}_0 > 1$. Our main result is that the stability of the endemic equilibrium depends on the number of stages: the endemic equilibrium is always stable when $n \leq 3$, while for any $n > 3$ it can be either stable or unstable, depending on the particular choice of the parameters. We generalize previous stability results for SIRS models as well and point out a mistake in the literature for multistage SEIRS models. Our results have important implications on the discretization of infectious periods with varying infectivity.

3.2 Model construction

In this Section, we investigate the stage progression SIS model

$$\begin{aligned}
S'(t) &= b(N(t)) + p_n I_n(t) - \sum_{k=1}^{n} \beta_k I_k(t) S(t) - \mu S(t), \\
I_1'(t) &= \sum_{k=1}^{n} \beta_k I_k(t) S(t) - p_1 I_1(t) - \mu I_1(t), \\
I_2'(t) &= p_1 I_1(t) - p_2 I_2(t) - \mu I_2(t), \\
&\vdots \\
I_n'(t) &= p_{n-1} I_{n-1}(t) - p_n I_n(t) - \mu I_n(t),
\end{aligned} \tag{3.1}$$

which describes the spread of a non-fatal infectious disease in a population with recruitment rate $b(N)$ and natural death rate μ. For simplicity, we will assume $b(N) = \mu N$, hence the

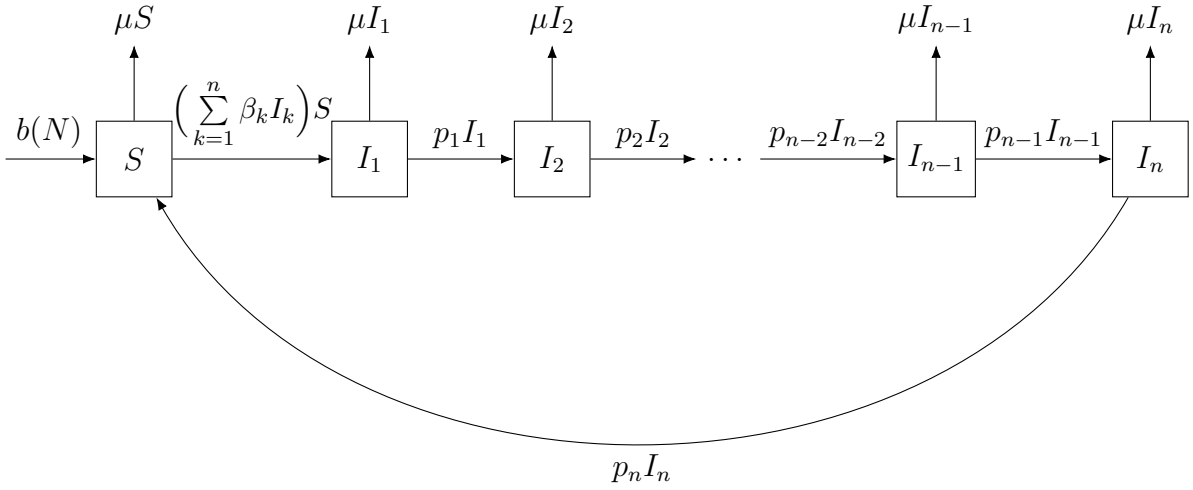

Figure 3.1: The transfer diagram of model (3.1).

total population $N(t) = S(t) + \sum_{j=1}^{n} I_j(t)$ will remain constant. Here, $S = S(t)$ represents the susceptible compartment, $I_1 = I_1(t), I_2 = I_2(t), \ldots, I_n = I_n(t)$ represent the infected compartments corresponding to stages $1, 2, \ldots, n$. We denote by β_i $(i = 1, 2, \ldots, n)$ the disease transmission rates in compartment I_i, and by p_i $(i = 1, 2, \ldots, n)$ the progression rates from disease stage i to $i+1$, i.e. from compartment I_i to I_{i+1}. We schematically depict the transfer diagram in Figure 3.1.

We normalize the constant population to unity ($N = 1$), hence the variables $S, I_1, \ldots, I_n$ represent the proportion of susceptible and infected individuals in the population, therefore we can write

$$S = 1 - \sum_{k=1}^{n} I_k. \tag{3.2}$$

Using (3.2) and decoupling the S equation, we obtain the n-dimensional system

$$\begin{aligned} I_1' &= \sum_{k=1}^{n} \beta_k I_k \left(1 - \sum_{k=1}^{n} I_k\right) - p_1 I_1 - \mu I_1, \\ I_2' &= p_1 I_1 - p_2 I_2 - \mu I_2, \\ &\vdots \\ I_n' &= p_{n-1} I_{n-1} - p_n I_n - \mu I_n. \end{aligned} \tag{3.3}$$

In the sequel, we analyse system (3.3) in details.

3.2.1 The basic reproduction number and the endemic equilibrium

First we calculate the basic reproduction number $\mathcal{R}_0$ for system (3.3). This is an important threshold parameter connected to the stability of the disease free equilibrium (DFE) and the existence of the endemic equilibrium (EE) for a large class of epidemic models, see [20] or

[22]. Here we use the next generation matrix method for calculating the basic reproduction number, following the notion of [33, 35]. We write the system (3.3) in the form of

$$\boldsymbol{I}' = \mathcal{F}(\boldsymbol{I}) - \mathcal{V}(\boldsymbol{I}),$$

where $\boldsymbol{I} = (I_1, I_2, \dots I_n)^T$ and

$$\mathcal{F} = (\mathcal{F}_1, \mathcal{F}_2, \dots \mathcal{F}_n)$$

represents the new infections, while

$$\mathcal{V} = (\mathcal{V}_1, \mathcal{V}_2, \dots \mathcal{V}_n)$$

contains the transitions between infected compartments. We linearize (3.3) at the DFE $(0, 0, \dots, 0)$ to obtain the equation

$$\boldsymbol{I}' = A\boldsymbol{I},$$

where A is the Jacobian matrix. Next, we take the decomposition $A = F - V$, where

$$F = \left[\frac{\partial \mathcal{F}_i}{\partial I_j}(DFE)\right], V = \left[\frac{\partial \mathcal{V}_i}{\partial I_j}(DFE)\right].$$

The obtained linearized system is

$$\begin{aligned} I_1' &= \sum_{k=1}^{n} \beta_k I_k - p_1 I_1 - \mu I_1, \\ I_2' &= p_1 I_1 - p_2 I_2 - \mu I_2, \\ &\vdots \\ I_n' &= p_{n-1} I_{n-1} - p_n I_n - \mu I_n, \end{aligned}$$

with

$$F = \begin{pmatrix} \beta_1 & \beta_2 & \dots & \beta_n \\ 0 & 0 & \dots & 0 \\ \vdots & \vdots & \ddots & \vdots \\ 0 & 0 & \dots & 0 \end{pmatrix}, \quad V = \begin{pmatrix} p_1 + \mu & 0 & \dots & 0 & 0 \\ -p_1 & p_2 + \mu & \dots & 0 & 0 \\ 0 & -p_2 & \ddots & \vdots & \vdots \\ \vdots & \vdots & \ddots & p_{n-1} + \mu & 0 \\ 0 & 0 & \dots & -p_{n-1} & p_n + \mu \end{pmatrix}.$$

The basic reproduction number $\mathcal{R}_0$ is the spectral radius $\rho(FV^{-1})$ of the next generation matrix FV^{-1}. It's easy to see that V^{-1} is a lower-triangular matrix, and all the elements of FV^{-1} are zero, except in its first row. Therefore its spectral radius is the only nonzero eigenvalue, that is

$$\mathcal{R}_0 = \sum_{k=1}^{n} \frac{\beta_k}{p_k + \mu} \left(\prod_{j=1}^{k-1} \frac{p_j}{p_j + \mu} \right). \tag{3.4}$$

Note that this expression for $\mathcal{R}_0$ matches the biological interpretation: taking a single infected individual, if we multiply the infection rate in stage k, the average time spent in stage k and the probability that the individual survives up to stage k, and sum up for all stages, we obtain (3.4).

Theorem 3.2.1. *For system* (3.3)*, a unique endemic equilibrium* $(I_1^*, I_2^*, \dots I_n^*)$ *(with* $I_k^* > 0$ *for all* $1 \le k \le n$*) exists if and only if* $\mathcal{R}_0 > 1$*. It is given by*

$$I_k^* = \frac{p_{k+1}+\mu}{p_k} \dots \frac{p_n+\mu}{p_{n-1}} \cdot \frac{1-\frac{1}{\mathcal{R}_0}}{Q}, \text{ where } Q = 1 + \frac{p_n+\mu}{p_{n-1}} + \dots + \prod_{i=1}^{n-1} \frac{p_{i+1}+\mu}{p_i}. \tag{3.5}$$

Proof. Setting the time derivatives zero in (3.3) yields

$$\begin{aligned} 0 &= \sum_{k=1}^{n} \beta_k I_k^* \left(1 - \sum_{k=1}^{n} I_k^*\right) - p_1 I_1^* - \mu I_1^*, \\ I_k^* &= \frac{p_{k+1}+\mu}{p_k} \cdot I_{k+1}^*, \quad k = 1, \dots, n-1. \end{aligned}$$

By iteration we find

$$I_k^* = \frac{p_{k+1}+\mu}{p_k} \dots \frac{p_n+\mu}{p_{n-1}} I_n^*. \tag{3.6}$$

If $I_n^* = 0$, then every $I_k^* = 0$, $k = 1, 2, \dots, n$. Now we assume that I_n^* is positive. Now we can see that

$$Q = \frac{I_n^*}{I_n^*} + \frac{I_{n-1}^*}{I_n^*} + \dots + \frac{I_1^*}{I_n^*} = \frac{\sum_{k=1}^{n} I_k^*}{I_n^*}. \tag{3.7}$$

We claim that

$$\sum_{k=1}^{n} \beta_k I_k^* = (p_1+\mu) \prod_{j=1}^{n-1} \frac{p_{j+1}+\mu}{p_j} \cdot I_n^* \cdot \mathcal{R}_0. \tag{3.8}$$

First we substitute (3.4) in $\mathcal{R}_0$, and then the coefficient of β_k in the right hand side is

$$(p_1+\mu) \prod_{j=1}^{n-1} \frac{p_{j+1}+\mu}{p_j} \cdot I_n^* \cdot \frac{1}{p_k+\mu} \prod_{l=1}^{k-1} \frac{p_l}{p_l+\mu}.$$

By (3.6), we find that it is indeed I_k^* and thus equation (3.8) holds. Substituting (3.8) into (3.6) and using (3.7), we find

$$(p_1+\mu) \prod_{k=1}^{n-1} \frac{p_{k+1}+\mu}{p_k} I_n^* \cdot (1 - I_n^* Q) \cdot \mathcal{R}_0 = (p_1+\mu) I_1^*.$$

From (3.6) with $k = 1$ and dividing by I_n^* we obtain

$$\frac{(p_1+\mu)(p_2+\mu)\dots(p_n+\mu)}{p_1 p_2 \dots p_{n-1}} (1 - I_n^* Q) \cdot \mathcal{R}_0 = \frac{(p_1+\mu)(p_2+\mu)\dots(p_n+\mu)}{p_1 p_2 \dots p_{n-1}}.$$

Therefore,

$$(1 - I_n^* Q) \cdot \mathcal{R}_0 = 1,$$

that is,

$$I_n^* = \frac{1-\frac{1}{\mathcal{R}_0}}{Q},$$

and substituting this into (3.6), the proof is completed. □

3.2.2 Threshold dynamics: disease extinction and persistence

We introduce the notation $D = \{\boldsymbol{I} \in \mathbb{R}^n_+ | \sum_{j=1}^n I_j \leq 1\}$ for the feasible phase space of model (3.3).

Theorem 3.2.2. *If $\mathcal{R}_0 \leq 1$ then the disease free equilibrium is globally asymptotically stable in the domain D, that is, the disease will be eradicated. If $\mathcal{R}_0 > 1$ then the disease persists uniformly in the population.*

Proof. We prove this result by following the methods of Theorem 2.1 and Theorem 2.2 from [33]. First we show that for system (3.3), the inequality

$$(F - V)\boldsymbol{I} \geq \mathcal{F}(\boldsymbol{I}) - \mathcal{V}(\boldsymbol{I})$$

holds for any $\boldsymbol{I} \in D$. Note that $V\boldsymbol{I} = \mathcal{V}(\boldsymbol{I})$. It's easy to see that in the first component of $\mathcal{F}$, the elements are multiplied by $1 - \sum_{k=1}^n I_k$, which is obviously less or equal than 1 in D. The first row of the matrix F does not contain this factor, so the linearized form $(F - V)\boldsymbol{I}$ is greater or equal than $\mathcal{F}(\boldsymbol{I}) - \mathcal{V}(\boldsymbol{I})$ for any $\boldsymbol{I} \in D$, with equality holding only at the DFE.

Let ω^T be the left eigenvector of the nonnegative matrix $V^{-1}F$ corresponding to the eigenvalue $\mathcal{R}_0 = \rho(V^{-1}F) = \rho(FV^{-1})$. The matrix V^{-1} is lower-trinagular and its nonzero elements are positive. The elements in the first row of F are all positive, and applying the rule of matrix multiplication, all elements of $V^{-1}F$ will be positive, and therefore, its adjacency matrix is strongly connected. Since FV^{-1} is irreducible and nonnegative, $\omega > 0$.

Consider $U := \omega^T V^{-1}\boldsymbol{I}$. Differentiation along solutions gives

$$\frac{dU}{dt} = \omega^T V^{-1}(\mathcal{F}(\boldsymbol{I}) - \mathcal{V}(\boldsymbol{I})) \leq \omega^T V^{-1}(F - V)\boldsymbol{I} = \omega^T V^{-1}F \cdot \boldsymbol{I} - \omega^T \cdot \boldsymbol{I} = (\mathcal{R}_0 - 1)\omega^T \cdot \boldsymbol{I}.$$

For $\mathcal{R}_0 < 1$, U is a Lyapunov function and the global asymptotic stability of the DFE in D follows. For $\mathcal{R}_0 = 1$, the same conclusion follows from LaSalle's invariance principle, noticing that in this case $\frac{dU}{dt} = 0$ implies $\mathcal{F}(\boldsymbol{I}) - \mathcal{V}(\boldsymbol{I}) = 0$, which holds if and only if $\boldsymbol{I}$ is an equilibrium. For $\mathcal{R}_0 = 1$, this can only be the DFE $(0, 0, \ldots, 0)$.

Now assume $\mathcal{R}_0 > 1$. For any $\epsilon > 0$, in the ϵ-neighborhood of the DFE we have $\mathcal{F}(\boldsymbol{I}) - \mathcal{V}(\boldsymbol{I}) \geq (F(1 - \epsilon) - V)\boldsymbol{I}$. Let $\epsilon > 0$ be so small that $\mathcal{R}_0(1 - \epsilon) > 1$ holds. Then, in this neighborhood,

$$\frac{dU}{dt} = \omega^T V^{-1}(\mathcal{F}(\boldsymbol{I}) - \mathcal{V}(\boldsymbol{I})) \geq \omega^T V^{-1}(F(1 - \epsilon) - V)\boldsymbol{I} = (\mathcal{R}_0(1 - \epsilon) - 1)\omega^T \cdot \boldsymbol{I} \geq 0.$$

We conclude that positive solutions can not converge to the DFE, and using standard arguments, the persistence result follows, thus there is an $\eta > 0$ such that for all positive solutions $\liminf_{t\to\infty} ||\boldsymbol{I}(t)|| > \eta$. □

3.3 Stability and instability

3.3.1 The endemic equilibrium is always stable for $n = 1, 2, 3$

The stability results are based on the Routh-Hurwitz-theorem, which we state below.

Theorem A. *For a given polynomial* $P(\lambda) = \lambda^n + a_1\lambda^{n-1} + ... + a_{n-1}\lambda + a_n$ *we define the Hurwitz-matrices*

$$H_1 = \begin{pmatrix} a_1 \end{pmatrix}, \; H_2 = \begin{pmatrix} a_1 & 1 \\ a_3 & a_2 \end{pmatrix}, \; H_3 = \begin{pmatrix} a_1 & 1 & 0 \\ a_3 & a_2 & a_1 \\ a_5 & a_4 & a_3 \end{pmatrix}, \ldots,$$

and

$$H_n = \begin{pmatrix} a_1 & 1 & 0 & 0 & \ldots & 0 \\ a_3 & a_2 & a_1 & 1 & \ldots & 0 \\ a_5 & a_4 & a_3 & a_2 & \ldots & 0 \\ \vdots & \vdots & \vdots & \vdots & \ddots & \vdots \\ 0 & 0 & 0 & 0 & \ldots & a_n \end{pmatrix},$$

where $a_j = 0$ *if* $j > n$. *All of the roots of* $P(\lambda)$ *are negative or have negative real part if and only if the determinants of all Hurwitz-matrices are positive:*

$$det\,(H_j) > 0 \text{ for all } j = 1, 2, \ldots, n.$$

Theorem 3.3.1. *If* $\mathcal{R}_0 > 1$ *and* $n = 1, 2, 3$, *then the endemic equilibrium is locally asymptotically stable.*

Proof. To apply the Routh-Hurwitz-theorem, we determine the Jacobian matrix and the characteristic polynomial $\chi(\lambda)$ of our system.

(a) $n = 1$: In this case our system is

$$I_1' = \beta_1 I_1 (1 - I_1) - p_1 I_1 - \mu I_1 = I_1(\beta_1 - p_1 - \mu - \beta_1 I_1). \tag{3.9}$$

Since $\mathcal{R}_0 > 1$ means $\beta_1 - p_1 - \mu > 0$, the stability of the positive equilibrium of this logistic equation is obvious.

(b) $n = 2$: In this case our system is

$$\begin{aligned} I_1' &= (\beta_1 I_1 + \beta_2 I_2)(1 - I_1 - I_2) - p_1 I_1 - \mu I_1, \\ I_2' &= p_1 I_1 - p_2 I_2 - \mu I_2, \end{aligned} \tag{3.10}$$

and the basic reproduction number is

$$\mathcal{R}_0 = \frac{\beta_1}{p_1 + \mu} + \frac{\beta_2 p_1}{(p_1 + \mu)(p_2 + \mu)} = \frac{\beta_1(p_2 + \mu) + \beta_2 p_1}{(p_1 + \mu)(p_2 + \mu)}. \tag{3.11}$$

The Jacobian of the system at the EE is the 2×2 matrix

$$\begin{pmatrix} \dfrac{\beta_1}{\mathcal{R}_0} - f - p_1 - \mu & \dfrac{\beta_2}{\mathcal{R}_0} - f \\ p_1 & -p_2 - \mu \end{pmatrix},$$

where

$$f = \sum_{k=1}^{2} \beta_k I_k^*. \tag{3.12}$$

The characteristic polynomial is

$$\begin{aligned}\chi(\lambda) =& \lambda^2 + \lambda \cdot \Big(2\mu + p_1 + p_2 + f - \frac{\beta_1}{\mathcal{R}_0}\Big) \\ &+ \Big(f\mu + fp_1 + fp_2 + \mu p_1 + \mu p_2 + p_1 p_2 + \mu^2 - \mu\frac{\beta_1}{\mathcal{R}_0} - p_1\frac{\beta_2}{\mathcal{R}_0} - p_2\frac{\beta_1}{\mathcal{R}_0}\Big).\end{aligned}$$

It's enough to prove that $\det(H_1) = a_1$ and $\det(H_2) = a_1 a_2$ are positive, which is equivalent to

(i) $a_1 > 0$,

(ii) $a_2 > 0$.

(i) We show that

$$f + 2\mu + p_1 + p_2 > \frac{\beta_1}{\mathcal{R}_0}.$$

Indeed, using (3.4) for $n = 2$, this is equivalent to

$$f + (p_2 + \mu) + (p_1 + \mu) > \frac{\beta_1(p_1 + \mu)(p_2 + \mu)}{\beta_1(p_2 + \mu) + \beta_2 p_1}.$$

If we multiply by the denominator of the right-hand side, we can clearly see that the left hand side is greater.

(ii) We have to prove that

$$f\mu + fp_1 + fp_2 + \mu p_1 + \mu p_2 + p_1 p_2 + \mu^2 - \mu\frac{\beta_1}{\mathcal{R}_0} - p_1\frac{\beta_2}{\mathcal{R}_0} - p_2\frac{\beta_1}{\mathcal{R}_0} > 0,$$

that is,

$$f\mu + fp_1 + fp_2 + (p_1 + \mu)(p_2 + \mu) > \mu\frac{\beta_1}{\mathcal{R}_0} + p_1\frac{\beta_2}{\mathcal{R}_0} + p_2\frac{\beta_1}{\mathcal{R}_0}. \tag{3.13}$$

Because of (3.11), it is true that

$$(p_1 + \mu)(p_2 + \mu) = (p_2 + \mu)\frac{\beta_1}{\mathcal{R}_0} + p_1\frac{\beta_2}{\mathcal{R}_0}.$$

If we subtract this from (3.13), we have $f\mu + fp_1 + fp_2 > 0$, and we conclude $a_2 > 0$.

(c) $n = 3$: In this case our system is

$$\begin{aligned} I_1' &= \sum_{k=1}^{3} \beta_k I_k \left(1 - \sum_{k=1}^{n} I_k\right) - p_1 I_1 - \mu I_1, \\ I_2' &= p_1 I_1 - p_2 I_2 - \mu I_2, \\ I_3' &= p_2 I_2 - p_3 I_3 - \mu I_3. \end{aligned} \tag{3.14}$$

The basic reproduction number is

$$\mathcal{R}_0 = \frac{\beta_1}{p_1 + \mu} + \frac{\beta_2 p_1}{(p_1 + \mu)(p_2 + \mu)} + \frac{\beta_3 p_1 p_2}{(p_1 + \mu)(p_2 + \mu)(p_3 + \mu)}. \tag{3.15}$$

We can easily deduce the Jacobian matrix

$$\begin{pmatrix} \frac{\beta_1}{\mathcal{R}_0} - f - p_1 - \mu & \frac{\beta_2}{\mathcal{R}_0} - f & \frac{\beta_3}{\mathcal{R}_0} - f \\ p_1 & -p_2 - \mu & 0 \\ 0 & p_2 & -p_3 - \mu \end{pmatrix},$$

where

$$f = \sum_{k=1}^{3} \beta_k I_k^*, \tag{3.16}$$

and

$$\begin{aligned} \chi(\lambda) = &- \lambda^3 - \lambda^2\Big(f + p_1 + p_2 + p_3 + 3\mu - \frac{\beta_1}{\mathcal{R}_0}\Big) \\ &- \lambda\Big(fp_1 + fp_2 + fp_3 + p_1p_2 + p_1p_3 + p_2p_3 + 2p_1\mu + 2p_2\mu + 2p_3\mu + 2f\mu \\ &+ 3\mu^2 - p_1\frac{\beta_2}{\mathcal{R}_0} - p_2\frac{\beta_1}{\mathcal{R}_0} - p_3\frac{\beta_1}{\mathcal{R}_0} - 2\mu\frac{\beta_1}{\mathcal{R}_0}\Big) \\ &- \Big(fp_1p_2 + fp_1p_3 + fp_2p_3 + p_1p_2p_3 + p_1p_2\mu + p_1p_3\mu + p_2p_3\mu \\ &+ fp_1\mu + fp_2\mu + fp_3\mu + f\mu^2 + p_1\mu^2 + p_2\mu^2 + p_3\mu^2 + \mu^3 \\ &- p_1p_2\frac{\beta_3}{\mathcal{R}_0} - p_1p_3\frac{\beta_2}{\mathcal{R}_0} - p_2p_3\frac{\beta_1}{\mathcal{R}_0} - p_1\frac{\beta_2}{\mathcal{R}_0}\mu - p_2\frac{\beta_1}{\mathcal{R}_0}\mu - p_3\frac{\beta_1}{\mathcal{R}_0}\mu - \frac{\beta_1}{\mathcal{R}_0}\mu^2\Big). \end{aligned}$$

We apply the Routh-Hurwitz criterion to -$\chi(\lambda)$, which has the same roots as $\chi(\lambda)$. It's enough to prove that

$$\det(H_1) = a_1, \quad \det(H_2) = a_1a_2 - a_3 \text{ and } \det(H_3) = a_3 \cdot (a_1a_2 - a_3)$$

are positive, which is equivalent to

(i) $a_1 > 0$,

(ii) $a_3 > 0$, and

(iii) $a_2 \cdot a_1 > a_3$.

(i) We show that

$$f + 3\mu + p_1 + p_2 + p_3 > \frac{\beta_1}{\mathcal{R}_0}. \tag{3.17}$$

Consider an equivalent form of (3.15):

$$(p_1+\mu)(p_2+\mu)(p_3+\mu) = (p_2+\mu)(p_3+\mu)\frac{\beta_1}{\mathcal{R}_0} + p_1(p_3+\mu)\frac{\beta_2}{\mathcal{R}_0} + p_1p_2\frac{\beta_3}{\mathcal{R}_0}. \tag{3.18}$$

Multiplying (3.17) with $\mathcal{R}_0$ and using (3.18), we obtain

$$\frac{\beta_3 p_1 p_2 + \beta_2 p_1(p_3+\mu) + \beta_1(p_2+\mu)(p_3+\mu)}{(p_1+\mu)(p_2+\mu)(p_3+\mu)}(f + 3\mu + p_1 + p_2 + p_3) > \beta_1. \tag{3.19}$$

Multiplying both sides with $(p_1+\mu)(p_2+\mu)(p_3+\mu)$, it is easy to see that the left hand side is greater.

(ii) From (3.18):

$$a_3 = f\mu^2 + f\mu p_1 + f p_1 p_2 + f p_1 p_3 + f\mu p_2 + f p_2 p_3 + f\mu p_3,$$

which is obviously positive.

(iii) It's enough to prove that the expression

$$\begin{aligned}
&\Big(-\frac{\beta_1}{\mathcal{R}_0} + f + 3\mu + p_1 + p_2 + p_3\Big)\Big(-2\frac{\beta_1}{\mathcal{R}_0}\mu + 2f\mu + fp_1 + fp_2 + fp_3 \\
&+ 3\mu^2 - \frac{\beta_2}{\mathcal{R}_0}p_1 + 2\mu p_1 + p_1p_2 + p_1p_3 - \frac{\beta_1}{\mathcal{R}_0}p_2 + 2\mu p_2 + p_2p_3 - \frac{\beta_1}{\mathcal{R}_0}p_3 + 2\mu p_3\Big) \\
&- \Big(f\mu^2 + f\mu p_1 + f p_1 p_2 + f p_1 p_3 + f\mu p_2 + f p_2 p_3 + f\mu p_3\Big)
\end{aligned}$$

is positive (we used (3.18) for a_3). This is equivalent to the inequality

$$\begin{aligned}
&\Big(-\frac{\beta_1}{\mathcal{R}_0} + f + 3\mu + p_1 + p_2 + p_3\Big)\Big(-2\frac{\beta_1}{\mathcal{R}_0}\mu + 2f\mu + fp_1 + fp_2 + fp_3 + 3\mu^2 \\
&- \frac{\beta_2}{\mathcal{R}_0}p_1 + 2\mu p_1 + p_1p_2 + p_1p_3 - \frac{\beta_1}{\mathcal{R}_0}p_2 + 2\mu p_2 + p_2p_3 - \frac{\beta_1}{\mathcal{R}_0}p_3 + 2\mu p_3\Big) \\
&> f\mu^2 + f\mu p_1 + f p_1 p_2 + f p_1 p_3 + f\mu p_2 + f p_2 p_3 + f\mu p_3.
\end{aligned}$$

Because of (3.18), obviously

$$(p_1+\mu)(p_2+\mu)(p_3+\mu) > (p_2+\mu)(p_3+\mu)\frac{\beta_1}{\mathcal{R}_0} + p_1(p_3+\mu)\frac{\beta_2}{\mathcal{R}_0},$$

and the even weaker inequality

$$(p_1+\mu)(p_2+\mu)(p_3+\mu) > (p_2+\mu)(p_3+\mu)\frac{\beta_1}{\mathcal{R}_0}$$

holds. Dividing these by $(p_3+\mu)$ and $(p_2+\mu)$, respectively, we find

$$(p_1+\mu)(p_2+\mu) > \frac{\beta_1}{\mathcal{R}_0}(p_2+\mu) + \frac{\beta_2}{\mathcal{R}_0}p_1, \tag{3.20}$$

and

$$(p_1+\mu)(p_3+\mu) > \frac{\beta_1}{\mathcal{R}_0}(p_3+\mu). \tag{3.21}$$

Considering (3.20) and (3.21), we can write

$$\begin{aligned}
&\Big(f+p_1+p_2+p_3+3\mu-\frac{\beta_1}{\mathcal{R}_0}\Big)\Bigg(2f\mu+fp_1+fp_2+fp_3+3\mu^2+2\mu p_1+p_1p_2\\
&+p_1p_3+2\mu p_2+p_2p_3+2\mu p_3-\Big(\frac{\beta_1}{\mathcal{R}_0}(p_2+\mu)+\frac{\beta_2}{\mathcal{R}_0}p_1+\frac{\beta_1}{\mathcal{R}_0}(p_3+\mu)\Big)\Bigg)\\
&>\Big(f+p_1+p_2+p_3+3\mu-\frac{\beta_1}{\mathcal{R}_0}\Big)\Big(2f\mu+fp_1+fp_2+fp_3+3\mu^2+2\mu p_1+p_1p_2\\
&+p_1p_3+2\mu p_2+p_2p_3+2\mu p_3\Big)-\big(p_1p_2+p_1\mu+p_2\mu+\mu^2+p_1p_3+\mu p_3+\mu p_1+\mu^2\big)\\
&=\Big(f+p_1+p_2+p_3+3\mu-\frac{\beta_1}{\mathcal{R}_0}\Big)\Big(fp_1+fp_2+fp_3+p_2p_3+2f\mu+p_2\mu+p_3\mu+\mu^2\Big).
\end{aligned}$$

We will prove that

$$\begin{aligned}
&\Big(f+p_1+p_2+p_3+3\mu-\frac{\beta_1}{\mathcal{R}_0}\Big)\Big(fp_1+fp_2+fp_3+p_2p_3+2f\mu+p_2\mu+p_3\mu+\mu^2\Big)\\
&>f\mu^2+f\mu p_1+fp_1p_2+fp_1p_3+f\mu p_2+fp_2p_3+f\mu p_3.
\end{aligned}$$

This is true if and only if

$$\begin{aligned}
&\Big(f+p_1+p_2+p_3+3\mu\Big)\Big(fp_1+fp_2+fp_3+p_2p_3+2f\mu+p_2\mu+p_3\mu+\mu^2\Big)\\
&>f\mu^2+f\mu p_1+fp_1p_2+fp_1p_3+f\mu p_2+fp_2p_3+f\mu p_3\\
&+\frac{\beta_1}{\mathcal{R}_0}\Big(fp_1+fp_2+fp_3+p_2p_3+2f\mu+p_2\mu+p_3\mu\Big).
\end{aligned}$$

From $p_1+\mu > \dfrac{\beta_1}{\mathcal{R}_0}$ which is an immediate implication of (3.15), it remained to prove that

$$\begin{aligned}
&\Big(f+p_1+p_2+p_3+3\mu\Big)\Big(fp_1+fp_2+fp_3+p_2p_3+2f\mu+p_2\mu+p_3\mu+\mu^2\Big)\\
&>f\mu^2+f\mu p_1+fp_1p_2+fp_1p_3+f\mu p_2+fp_2p_3+f\mu p_3\\
&+(p_1+\mu)\Big(fp_1+fp_2+fp_3+p_2p_3+2f\mu+p_2\mu+p_3\mu+\mu^2\Big).
\end{aligned}$$

Expanding both sides, one can easily see that the left-hand side is greater indeed.

□

3.3.2 Dynamics in higher dimensions: the endemic equilibrium can be either stable or unstable for any $n \geq 4$

Stable case

We prove first that the endemic equilibrium can be stable in (3.3) for any $n \geq 4$, with suitable parameters β_i, p_i and μ. Let us set in (3.3) $\beta := \beta_1 = \beta_2 = \cdots = \beta_n$, and $p := p_1 = \dots p_n$, and $\mu = 0$. Then we have

$$\begin{aligned} I_1' &= \beta \sum_{k=1}^{n} I_k \left(1 - \sum_{k=1}^{n} I_k\right) - pI_1, \\ I_2' &= pI_1 - pI_2, \\ &\vdots \\ I_n' &= pI_{n-1} - pI_n. \end{aligned} \tag{3.22}$$

From (3.4) and (3.5), we obtain the basic reproduction number and the EE as

$$\mathcal{R}_0 = \frac{\beta \cdot n}{p}, \quad I_1^* = I_2^* = \cdots = I_n^* = \frac{1 - \frac{p}{\beta n}}{n}. \tag{3.23}$$

Theorem 3.3.2. *The characteristic polynomial of (3.22) at the EE is*

$$\chi_n(\lambda) = (-1)^n \left((p+\lambda)^n + \left(\beta - \frac{2p}{n}\right) \cdot \sum_{i=0}^{n-1} (p+\lambda)^i \cdot p^{n-1-i} \right). \tag{3.24}$$

Proof. We use the notation $[(p+\lambda)^i][X]$ for the coefficient of $(p+\lambda)^i$ in some expression X. With such a notation, we will prove by induction that

$$[(p+\lambda)^i][\chi_n(\lambda)] = \begin{cases} (-1)^n, & i = n \\ (-1)^n \cdot \left(\beta - \frac{2p}{n}\right) \cdot p^{n-1-i}, & i = 0, 1, \dots, n-1. \end{cases}$$

From (3.22) and (3.23) we obtain the $n \times n$-size characteristic matrix

$$D_n(\lambda) = \begin{pmatrix} \frac{2p}{n} - \beta - p - \lambda & \frac{2p}{n} - \beta & \frac{2p}{n} - \beta & \dots & \frac{2p}{n} - \beta \\ p & -p - \lambda & 0 & \dots & 0 \\ 0 & p & -p - \lambda & \dots & 0 \\ \vdots & \vdots & \vdots & \ddots & \vdots \\ 0 & 0 & 0 & \dots & -p - \lambda \end{pmatrix},$$

and we look for it's determinant. One can easily check the $n = 1$ case. If we expand $|D_n(\lambda)|$ by the last column, we find

$$\chi_n(\lambda) = |D_n(\lambda)| = (-1) \cdot (p+\lambda) \cdot |C_{n-1}(\lambda)| + (-1)^{n+1} \left(\frac{2p}{n} - \beta\right) \cdot p^{n-1}, \tag{3.25}$$

where

$$C_{n-1}(\lambda) = \begin{pmatrix} \frac{2p}{n} - \beta - p - \lambda & \frac{2p}{n} - \beta & \frac{2p}{n} - \beta & \cdots & \frac{2p}{n} - \beta \\ p & -p - \lambda & 0 & \cdots & 0 \\ \vdots & \vdots & \vdots & \vdots & \vdots \\ 0 & 0 & \cdots & p & -p - \lambda \end{pmatrix} \in \mathbb{R}^{(n-1)\times(n-1)}.$$

From the Leibniz formula of computing determinants, we deduce

$$[(p+\lambda)^i][|C_{n-1}(\lambda)|] = \begin{cases} (-1)^{n-1}, & i = n-1 \\ [(p+\lambda)^i][|D_{n-1}(\lambda)|] \cdot \frac{\beta - \frac{2p}{n}}{\beta - \frac{2p}{n-1}}, & i = 0, 1, \ldots, n-2. \end{cases}$$

Combining this with (3.25) and using the induction hypothesis for $n-1$, we arrive at

$$[(p+\lambda)^i][\chi_n(\lambda)] = \begin{cases} (-1)^n, & i = n \\ (-1)^n p^{n-1-i} \cdot \left(\beta - \frac{2p}{n}\right), & i = 0, 1, \ldots, n-1. \end{cases}$$

□

Theorem 3.3.3. *The endemic equilibrium of (3.22) is stable.*

Proof. We prove first that for $1 < \mathcal{R}_0 \leq 2$ the characteristic equation does not have a root with positive real part. Substituting $\alpha + i\omega$ with $\alpha > 0$ to the characteristic equation $\chi_n(\lambda) = 0$ and dividing by the non-zero $(p + \alpha + i\omega)^n$ yield

$$1 = \left(\frac{2p}{n} - \beta\right) \cdot \left(\frac{1}{p+\alpha+i\omega} + \frac{p}{(p+\alpha+i\omega)^2} + \cdots + \frac{p^{n-1}}{(p+\alpha+i\omega)^n}\right). \tag{3.26}$$

Taking the absolute value of both sides, we get

$$1 = \left(\frac{2p}{n} - \beta\right) \cdot \left|\frac{1}{p+\alpha+i\omega} + \frac{p}{(p+\alpha+i\omega)^2} + \cdots + \frac{p^{n-1}}{(p+\alpha+i\omega)^n}\right|, \tag{3.27}$$

because $1 < \mathcal{R}_0 \leq 2$ implies the nonnegativity of $\dfrac{2p}{n} - \beta$. The right-hand side is clearly smaller than

$$n \cdot \left|\frac{1}{p+\alpha+i\omega}\right|,$$

so

$$1 < n\left(\frac{2p}{n} - \beta\right)\left|\frac{1}{p+\alpha+i\omega}\right| = (2p - \beta n)\left|\frac{1}{p+\alpha+i\omega}\right|. \tag{3.28}$$

Since $\mathcal{R}_0 > 1$ implies $\beta n > p$, we have $(2p - \beta n) < p$ and thus

$$1 < (2p - \beta n)\left|\frac{1}{p+\alpha+i\omega}\right| < p\left|\frac{1}{p+\alpha+i\omega}\right| < 1 \tag{3.29}$$

whenever $\alpha > 0$, which is a contradiction.

The next step is to prove that (3.24) does not have a root $i\omega$ with $\omega > 0$ for any $\mathcal{R}_0 > 1$. Substituting $i\omega$ to $\chi_n(\lambda) = 0$ and dividing by $(p + i\omega)^n$ we derive

$$1 = \left(\frac{2p}{n} - \beta\right) \cdot \left(\frac{1}{p + i\omega} + \frac{p}{(p + i\omega)^2} + \cdots + \frac{p^{n-1}}{(p + i\omega)^n}\right) = \left(\frac{2p}{n} - \beta\right) \cdot \frac{1 - \left(\frac{p}{p + i\omega}\right)^n}{i\omega}. \quad (3.30)$$

This implies

$$i\omega - \left(\frac{2p}{n} - \beta\right) = (-1) \cdot \left(\frac{2p}{n} - \beta\right) \cdot \left(\frac{p^n}{(p + i\omega)^n}\right). \quad (3.31)$$

Taking the absolute value of both sides yields

$$\left| i\omega - \left(\frac{2p}{n} - \beta\right) \right| = \left| \left(\frac{2p}{n} - \beta\right) \right| \cdot \left| \frac{p^n}{(p + i\omega)^n} \right|, \quad (3.32)$$

and there is a contradiction, because of $\omega > 0$, the left-hand side is greater than $|\frac{2p}{n} - \beta|$ and the right-hand side is less than $|\frac{2p}{n} - \beta|$. This implies the stability of the equilibrium because the eigenvalues are depending continuously on the characteristic equation (see [30]). Since the endemic equilibrium is stable for $\mathcal{R}_0 \leq 2$, if it would be unstable for some (β, n, p) configuration, there must be a configuration with purely imaginary root $i\omega$ as well, which is not possible. □

Unstable case

We have seen that the endemic equilibrium in system (3.3) can be stable. Now we would like to show that one can choose the parameters such that the endemic equilibrium will be unstable, therefore we can discover oscillation in the dynamics. We will set now in (3.3) $\beta_1 = \beta > 0$, $\beta_2 = \beta_3 = \cdots = \beta_n = 0$, $p_1 = p > 0$, $p_2 = p_3 = \cdots = p_n = q > 0$ and $\mu = 0$, this means we reduced (3.3) to

$$\begin{aligned} I_1' &= \beta I_1 \left(1 - \sum_{k=1}^{n} I_k\right) - pI_1, \\ I_2' &= pI_1 - qI_2, \\ I_3' &= qI_2 - qI_3, \\ &\vdots \\ I_n' &= qI_{n-1} - qI_n. \end{aligned} \quad (3.33)$$

It is easy to calculate the basic reproduction number as $\mathcal{R}_0 = \dfrac{\beta}{p}$. The endemic equilibrium satisfies $I_2^* = \cdots = I_n^* = \frac{p}{q} I_1^*$, and substituting to the first equation yields

$$I_1^* = \frac{1 - \frac{p}{\beta}}{(n-1)\frac{p}{q} + 1}, \quad I_2^* = \cdots = I_n^* = \frac{p}{q} \frac{1 - \frac{p}{\beta}}{(n-1)\frac{p}{q} + 1}. \quad (3.34)$$

Theorem 3.3.4. *The characteristic polynomial of (3.33) is*

$$\chi_n(\lambda) = (-1)^n\bigg((q+\lambda)^{n-1}(\beta\cdot I_1^*+\lambda)+\frac{p\cdot\beta\cdot I_1^*}{\lambda}\Big((q+\lambda)^{n-1}-q^{n-1}\Big)\bigg). \tag{3.35}$$

Proof. We prove this by induction. One can easily check the base case $n = 1$. For the induction step, assume that (3.35) holds for some n, and our goal is to show

$$\chi_{n+1}(\lambda) = (-1)^{n+1}\bigg((q+\lambda)^{n}(\beta\cdot I_1^*+\lambda)+\frac{p\cdot\beta\cdot I_1^*}{\lambda}\Big((q+\lambda)^{n}-q^{n}\Big)\bigg).$$

We have to compute the following determinant:

$$\chi_{n+1}(\lambda) = \begin{vmatrix} -\beta\cdot I_1^*-\lambda & -\beta\cdot I_1^* & -\beta\cdot I_1^* & -\beta\cdot I_1^* & \cdots & -\beta\cdot I_1^* & -\beta\cdot I_1^* \\ p & -q-\lambda & 0 & 0 & \cdots & 0 & 0 \\ 0 & q & -q-\lambda & 0 & \cdots & 0 & 0 \\ 0 & 0 & q & -q-\lambda & \cdots & 0 & 0 \\ \vdots & \vdots & \vdots & \vdots & \ddots & \vdots & \vdots \\ 0 & 0 & 0 & \cdots & q & -q-\lambda & 0 \\ 0 & 0 & 0 & \cdots & 0 & q & -q-\lambda \end{vmatrix}.$$

We start to expand it by the last column:

$$\chi_{n+1}(\lambda) = (-1)(q+\lambda)\chi_n(\lambda) + (-1)^{n+1}(\beta\cdot I_1^*)\cdot p\cdot q^{n-1}.$$

Using (3.35) yields

$$\begin{aligned}\chi_{n+1}(\lambda) = (-1)^{n+1}\bigg((q+\lambda)^{n}(\beta\cdot I_1^*+\lambda)\bigg) + (-1)^{n+1}(q+\lambda)\frac{p\cdot\beta\cdot I_1^*}{\lambda}\bigg((q+\lambda)^{n-1}-q^{n-1}\bigg) \\ + (-1)^{n+1}\beta\cdot I_1^*\cdot p\cdot q^{n-1}.\end{aligned}$$

Notice that

$$(q+\lambda)\frac{p\cdot\beta\cdot I_1^*}{\lambda}\bigg((q+\lambda)^{n-1}-q^{n-1}\bigg) = \frac{p\cdot\beta\cdot I_1^*}{\lambda}(q+\lambda)^n - \frac{p\cdot\beta\cdot I_1^*}{\lambda}q^n - p\cdot\beta\cdot I_1^*\cdot q^{n-1},$$

Removing the parentheses,

$$\begin{aligned}\chi_{n+1}(\lambda) = (-1)^{n+1}(q+\lambda)^n(\beta\cdot I_1^*+\lambda) + \frac{p\cdot\beta\cdot I_1^*}{\lambda}(-1)^{n+1}\cdot(q+\lambda)^n \\ + \frac{p\cdot\beta\cdot I_1^*}{\lambda}(-1)^n q^{n-1}(q+\lambda) + (-1)^{n+1}\beta\cdot I_1^*\cdot p\cdot q^{n-1},\end{aligned}$$

and

$$\chi_{n+1}(\lambda) = (-1)^{n+1}(q+\lambda)^n(\beta\cdot I_1^*+\lambda) + \frac{p\cdot\beta\cdot I_1^*}{\lambda}(-1)^{n+1}(q+\lambda)^n + \frac{p\cdot\beta\cdot I_1^*}{\lambda}(-1)^n q^n + \Theta,$$

where

$$\Theta = (-1)^n\cdot p\cdot\beta\cdot I_1^*\cdot q^{n-1} + (-1)^{n+1}\cdot p\cdot\beta\cdot I_1^*\cdot q^{n-1} = 0.$$

Now we have

$$\chi_{n+1}(\lambda) = (-1)^{n+1}\bigg((q+\lambda)^n(\beta\cdot I_1^* + \lambda) + \frac{p\cdot\beta\cdot I_1^*}{\lambda}\Big((q+\lambda)^n - q^n\Big)\bigg),$$

and the induction step is completed. □

We will prove that $\chi_n(\lambda)$ has pure imaginary roots $\lambda = i\omega$. With the notation $\frac{p}{q} = \alpha, \frac{\lambda}{q} = z$ and using $\frac{\beta}{p} = \mathcal{R}_0$, after some manipulation we can write $\chi_n(\lambda) = 0$ in the form

$$z + \frac{\alpha\cdot(\mathcal{R}_0-1)}{(n-1)\cdot\alpha+1} + \frac{\alpha}{z}\cdot\frac{\alpha\cdot(\mathcal{R}_0-1)}{(n-1)\cdot\alpha+1}\left(1 - \frac{1}{(z+1)^{n-1}}\right) = 0. \tag{3.36}$$

Substituting $z = i\omega$ yields

$$i\omega + \frac{\alpha\cdot(\mathcal{R}_0-1)}{(n-1)\cdot\alpha+1} - i\frac{\alpha}{\omega}\cdot\frac{\alpha\cdot(\mathcal{R}_0-1)}{(n-1)\cdot\alpha+1}\left(1 - \frac{1}{(i\omega+1)^{n-1}}\right) = 0. \tag{3.37}$$

The real and imaginary parts of this equation are

(i) $$\frac{\alpha\cdot(\mathcal{R}_0-1)}{(n-1)\cdot\alpha+1} - \frac{\alpha}{\omega}\cdot\frac{\alpha\cdot(\mathcal{R}_0-1)}{(n-1)\cdot\alpha+1}\cdot\operatorname{Im}\left(\frac{1}{(i\omega+1)^{n-1}}\right) = 0,$$

(ii) $$\omega^2 = \alpha\cdot\frac{\alpha\cdot(\mathcal{R}_0-1)}{(n-1)\cdot\alpha+1}\left(1 - \operatorname{Re}\left(\frac{1}{(i\omega+1)^{n-1}}\right)\right).$$

Solving these equations for α and $\sigma := \mathcal{R}_0 - 1$, we find

$$\begin{aligned}\alpha &= \frac{\omega}{\operatorname{Im}\left(\frac{1}{(i\omega+1)^{n-1}}\right)},\\ \sigma &= \frac{\operatorname{Im}\left(\frac{1}{(i\omega+1)^{n-1}}\right)\left((n-1)\cdot\omega + \operatorname{Im}\left(\frac{1}{(i\omega+1)^{n-1}}\right)\right)}{1 - \operatorname{Re}\left(\frac{1}{(i\omega+1)^{n-1}}\right)}.\end{aligned} \tag{3.38}$$

Theorem 3.3.5. *For every $n \geq 4$ there is a suitable $\omega > 0$, $\alpha > 1$ and $\sigma > 0$ that solves* (3.38) *and the transversality condition Re $z'(\sigma) \neq 0$ is satisfied for (3.36). Therefore a Hopf bifurcation occurs, and the endemic equilibrium can be unstable.*

Proof. Using

$$\operatorname{Re}\left(\frac{1}{(i\omega+1)^{n-1}}\right) = \frac{\cos\left((n-1)\cdot\arctan\omega\right)}{(1+\omega^2)^{\frac{n-1}{2}}}, \tag{3.39}$$

and

$$\operatorname{Im}\left(\frac{1}{(i\omega+1)^{n-1}}\right) = -\frac{\sin\left((n-1)\cdot\arctan\omega\right)}{(1+\omega^2)^{\frac{n-1}{2}}}, \tag{3.40}$$

it is clear that $-1 < \operatorname{Re}\left(\frac{1}{(i\omega+1)^{n-1}}\right) < 1$, so whenever

$$0 < \operatorname{Im}\left(\frac{1}{(i\omega+1)^{n-1}}\right) < \omega \tag{3.41}$$

holds, from (3.38) we can see that $\alpha > 1$ and $\sigma > 0$. We confirm that

$$\omega = \tan\left(\frac{5\pi}{12}\right) \text{ is suitable for } n = 4, \tag{3.42}$$
$$\omega = \tan\left(\frac{\pi}{n-2}\right) \text{ is suitable for every } n > 4.$$

In the case $n = 4$, using (3.40),

$$\mathrm{Im}\left(\frac{1}{(i\omega+1)^{n-1}}\right) = -\sin\left(\frac{15\pi}{12}\right)\cdot\cos^3\left(\frac{5\pi}{12}\right) = \frac{(\sqrt{3}-1)^3}{32},$$

which is positive, but smaller than $\tan\left(\frac{5\pi}{12}\right) = 2+\sqrt{3}$. Similarly, for $n > 4$,

$$\mathrm{Im}\left(\frac{1}{(i\omega+1)^{n-1}}\right) = -\sin\left(\frac{(n-1)\pi}{n-2}\right)\cdot\cos^{n-1}\left(\frac{\pi}{n-2}\right).$$

Since $-\sin\left(\frac{(n-1)\pi}{n-2}\right) = \sin\left(\frac{\pi}{n-2}\right) < \tan\left(\frac{\pi}{n-2}\right)$, (3.41) holds.

We found that for $n \geq 4$, purely imaginary roots may exist. Implicit differentiation of

$$G(z(\sigma),\sigma) := z + \frac{\alpha\cdot\sigma}{(n-1)\cdot\alpha+1} + \frac{\alpha}{z}\cdot\frac{\alpha\cdot\sigma}{(n-1)\cdot\alpha+1}\left(1-\frac{1}{(z+1)^{n-1}}\right) = 0$$

shows that $\mathrm{Re}\ z'(\sigma) \neq 0$ if and only if

$$\mathrm{Re}\left(-\frac{\partial G}{\partial\sigma}\Big/\frac{\partial G}{\partial z}\right) \neq 0.$$

Noting that

$$\frac{\partial G}{\partial\sigma} = \frac{G-z}{\sigma} = -\frac{z}{\sigma},$$

and

$$\frac{\partial G}{\partial z} = 1 - \frac{1}{z}\cdot\left(-z - \frac{\alpha\sigma}{(n-1)\cdot\alpha+1}\right) + \frac{\alpha}{z}\cdot\frac{\alpha\sigma}{(n-1)\cdot\alpha+1}(n-1)\cdot\frac{1}{(1+z)^n},$$

at $z = i\omega$ it is enough to show that

$$\mathrm{Im}\frac{\partial G}{\partial z} = -\frac{\alpha\sigma}{(n-1)\cdot\alpha+1}\cdot\frac{1}{\omega} - \frac{\alpha}{\omega}\frac{\alpha\sigma}{(n-1)\cdot\alpha+1}(n-1)\frac{\cos(n\arctan\omega)}{(1+\omega^2)^{\frac{n}{2}}} \neq 0.$$

We can divide by the nonzero $\dfrac{\alpha\sigma}{(n-1)\cdot\alpha+1}\cdot\dfrac{1}{\omega}$ to obtain

$$-1 - \alpha\cdot(n-1)\cdot\frac{\cos(n\arctan\omega)}{(1+\omega^2)^{\frac{n}{2}}} \neq 0. \tag{3.43}$$

In the case of $n = 4$, the left hand side is

$$-1 + \frac{3\sin\left(\frac{5\pi}{12}\right)}{\sin\left(\frac{15\pi}{12}\right)\cos^3\left(\frac{5\pi}{12}\right)}\cdot\cos\left(\frac{20\pi}{12}\right)\cdot\cos^4\left(\frac{5\pi}{12}\right) = -1 - \frac{3}{4\sqrt{2}}.$$

If $n > 4$, we get from (3.38) and (3.42) that $\alpha = \dfrac{1}{\cos^n\left(\frac{\pi}{n-2}\right)}$, so we can write (3.43) as

$$-1 - (n-1) \cdot \cos\left(\frac{n}{n-2}\pi\right) \neq 0.$$

This is equivalent to

$$\cos\left(\frac{2\pi}{n-2}\right) \neq \frac{1}{n-1},$$

and one can check by elementary calculus that this holds for any integer $n \geq 5$. □

4

Instability in an SEIRS model

In [31], the transmission dynamics of an $SEIRS$ model was investigated for an infectious disease with n infectious stages, given by the system

$$\begin{aligned} S' &= \pi + \theta R - \sum_{k=1}^{n} \frac{\beta_k I_k}{N} S - \mu_S S, \\ E' &= \sum_{k=1}^{n} \frac{\beta_k I_k}{N} S - \sigma_E E - \mu_E E, \\ I_1' &= \sigma_E E - \sigma_1 I_1 - \mu_1 I_1 - \delta_1 I_1, \\ I_j' &= \sigma_{j-1} I_{j-1} - \sigma_j I_j - \mu_j I_j - \delta_j I_j, ; \quad j = 2, 3, \ldots, n \\ R' &= \sigma_n I_n - \theta R - \mu_R R, \end{aligned} \tag{4.1}$$

where π is the recruitment rate of susceptible individuals into the population, θ is the rate of the loss of immunity among recovered individuals, β_k are the effective contact rates and $\sigma_E, \sigma_{I_k}, \ \mu_S, \mu_E, \mu_{I_k}, \mu_R, \delta_k \ (k = 1, 2, \ldots, n)$ describe per capita rates of disease progression, natural death and disease-induced death, respectively. We assume that all these parameters are nonnegative. We denote by N the total population ($N = S + E + \sum_{k=1}^{n} I_k + R$), by E the compartment of exposed individuals, by I_j the compartment of infected individuals in disease stage j, and by R the compartment of recovered and immune individuals. By applying a similar method as in Theorem 3.3.5, we can show that the endemic equilibrium can be unstable. In [31], the authors formulated Conjecture 1 about the global asymptotic stability of the endemic equilibrium. Consequently, in light of Proposition 4.0.1, this conjecture is also disproved, which can also be illustrated by the periodic solution in Figure 4.1.

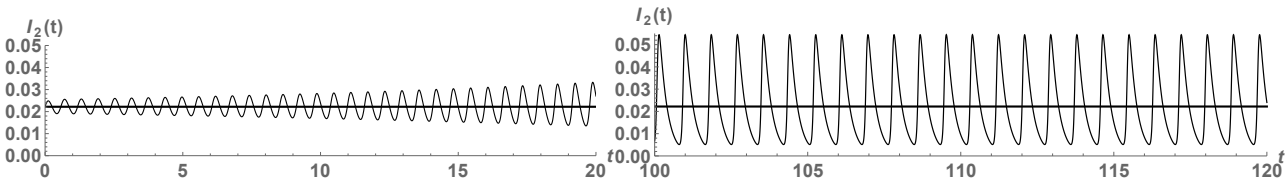

Figure 4.1: Snapshots of an oscillatory solution of system (4.3) with parameter configuration (4.5), with $t \in [0, 20]$ (in the left) and $t \in [100, 120]$ (in the right).

Proposition 4.0.1. *There exist a parameter set for (4.1) such that the endemic equilibrium exists and it is unstable.*

Proof. Let $n = 3$ and set

$$\begin{aligned} &\pi = 0, N = 1, \mu_S = \mu_E = \mu_1 = \mu_2 = \mu_3 = \mu_R = 0, \sigma_E = p, \\ &\sigma_1 = q, \sigma_2 = \sigma_3 = \theta = r, \beta_2 = \beta_3 = 0. \end{aligned} \tag{4.2}$$

Normalizing the constant population size to unity, we can omit S from the system to get

$$\begin{aligned} E' &= \beta_1 I_1 \left(1 - E - \sum_{k=1}^{3} I_k - R\right) - pE, \\ I_1' &= pE - qI_1, \\ I_2' &= qI_1 - rI_2, \\ I_3' &= rI_2 - rI_3, \\ R' &= rI_3 - rR. \end{aligned} \tag{4.3}$$

Using (3.4) and (3.5) to calculate the positive equilibrium and $\mathcal{R}_0$, we find

$$E^* = \frac{r}{p}\frac{\frac{\beta_1}{q} - 1}{\frac{\beta_1}{q}(\frac{r}{p} + 3 + \frac{r}{q})},\ I_1^* = \frac{r}{q}\frac{\frac{\beta_1}{q} - 1}{\frac{\beta_1}{q}(\frac{r}{p} + 3 + \frac{r}{q})},\ I_2^* = I_3^* = R^* = \frac{\frac{\beta_1}{q} - 1}{\frac{\beta_1}{q}(\frac{r}{p} + 3 + \frac{r}{q})} \text{ and } \mathcal{R}_0 = \frac{\beta_1}{q}.$$

One can easily compute the characteristic matrix

$$C = \begin{pmatrix} \frac{r}{q}\frac{q-\beta_1}{3+\frac{r}{p}+\frac{r}{q}} - p - \lambda & q + \frac{r}{q}\frac{q-\beta_1}{3+\frac{r}{p}+\frac{r}{q}} & \frac{r}{q}\frac{q-\beta_1}{3+\frac{r}{p}+\frac{r}{q}} & \frac{r}{q}\frac{q-\beta_1}{3+\frac{r}{p}+\frac{r}{q}} & \frac{r}{q}\frac{q-\beta_1}{3+\frac{r}{p}+\frac{r}{q}} \\ p & -q - \lambda & 0 & 0 & 0 \\ 0 & q & -r - \lambda & 0 & 0 \\ 0 & 0 & r & -r - \lambda & 0 \\ 0 & 0 & 0 & r & -r - \lambda \end{pmatrix}.$$

If we denote $\frac{r}{q}\frac{q-\beta_1}{3+\frac{r}{p}+\frac{r}{q}}$ by s, the characteristic polynomial can be written as

$$|C| = A_1 \cdot \lambda^5 + A_2 \cdot \lambda^4 + A_3 \cdot \lambda^3 + A_4 \cdot \lambda^2 + A_5 \cdot \lambda + A_6, \tag{4.4}$$

where

$$\begin{aligned} A_1 &= -1, \\ A_2 &= -p - q - 3r + s, \\ A_3 &= -3pr - 3qr - 3r^2 + ps + qs + 3rs, \\ A_4 &= -3pr^2 - 3qr^2 - r^3 + pqs + 3prs + 3qrs + 3r^2 s, \\ A_5 &= -pr^3 - qr^3 + 3pqrs + 3pr^2 s + 3qr^2 s + r^3 s, \\ \text{and } A_6 &= 3pqr^2 s + pr^3 s + qr^3 s. \end{aligned}$$

Setting

$$\beta_1 = 1500,\ q = 1400,\ p = 5000 \text{ and } r = 4, \tag{4.5}$$

we have eigenvalues

$$\lambda_1 \approx 0.0616677 - 10.5925i,$$
$$\lambda_2 \approx 0.0616677 + 10.5925i,$$

hence, the endemic equilibrium is unstable and there is oscillation in the dynamics (see Figure (4.1)). From the continuous dependence of the eigenvalues on parameters (see [30]), we find that instability is possible when all parameters are positive as well. □

This proposition contradicts Theorem 3 of [31], which stated that the endemic equilibrium of system (4.1) is always locally asymptotically stable, therefore that theorem seems to be false. In this Theorem the authors apply the Krasnoselskii sub-linearity trick, which is a common approach to prove the local stability of the endemic equilibrium. We refer to Hethcote and Thieme [25] for the explanation of this method.

The method is, if $x' = f(x)$ is an $n \times n$ system of differential equations and $\overline{x} \in \mathbb{R}^n$ is an equilibrium point, then the linearized equation

$$\mathbf{Z}'(t) = Mf(\bar{x})\mathbf{Z}$$

has no solution with the form of

$$\mathbf{Z}(t) = \mathbf{Z}_0 e^{\omega t}$$

with $\mathbf{Z}_0 \in \mathbb{C}\backslash\{0\}, \mathbf{Z}_0 = (Z_0, Z_1, \ldots, Z_m, Z_{m+1}), Z_i \in \mathbb{C}, \omega \in \mathbb{C}$ and $\mathrm{Re}(\omega) \geqslant 0$.

When authors derive the proof of local stability, an important technical step is to ensure that if $\mathrm{Re}(\omega) > 0$ holds then $\mathrm{Re}(\mu(\omega)) > 0$ also stands for some function $\mu(\omega)$. In various papers, however, authors use this method for a function of the form

$$\mu(\omega) = \frac{1}{(\omega + k_0) \cdot (\omega + k_1)}$$

with $k_0, k_1 \in \mathbb{R}$. This can have a negative real part, for example $\omega = 1 + 4i, z_0 = z_1 = 1$. Overall, we found 14 published papers in the literature with such an incorrect application of Krasnoselskii's method.

5

Dynamics of a COVID-type model with symptom-based testing

5.1 Model construction

In this work, we consider an extended $SEIR$-type compartmental model for the transmission dynamics of COVID-19. We incorporate symptom-based testing of patients and isolation upon positive result *i.e.* removal from the infectious chain. The clinical symptoms that trigger the testing of individuals is referred to as *indicator symptom*. The *force of testing* is defined as the rate at which infected individuals are tested, see Sect. 5.2. It is described by a nonlinear function of the state of the epidemic and of all individuals displaying the indicator symptom at a given time, with or without COVID-19 infection, hence, it is considerably different from previous approaches. Our goal is to understand the impact, and especially the limitations of this testing strategy, hence we model neither contact-tracing of patients with positive tests nor the testing of a fraction of non-symptomatic contacts, both of which are common and efficient improvements and result in removal of additional patients from the infectious chain. Moreover, we assume perfect testing, that is we do not consider false positive or false negative results.

According to the current understanding of the disease, none of the symptoms are specific solely for COVID-19, thus, the chosen indicator symptom may and will be present amongst other individuals not infected with SARS-CoV-2. All patients, with or without COVID-19 infection, displaying the indicator symptom form the so-called *primary symptom pool*, whilst, those without COVID-19 infection (but with the same indicator symptom) are members of the *secondary symptom pool*, see Sect. 5.2. Naturally, choosing the indicator symptom for a testing campaign should be affected by its prevalence and by the historical statistics for the size of the associated secondary symptom pool. We emphasize that the latter might undergo seasonal variations as is typical with respiratory symptoms peaking in influenza season [11]. This is a common but not uniform feature of COVID-19 symptoms, *e.g.* gastrointestinal symptoms might show no seasonal variations, depending on age-groups [12].

The chapter is structured as follows. Sect. 5.2 presents the compartmental epidemic model and its parametrization. In addition, the next generation matrix computations are included that are used to derive formulae for the reproduction number. Then, Sect. 5.3

establishes several boundedness and monotonicity-type results on key characteristics of the epidemic model. The results of numerical simulations are discussed in Sect. 5.4.

5.2 The epidemic model of indicator symptom-based testing

To assess the effectiveness of indicator symptom based testing in controlling the spread of COVID-19, we developed a compartmental population model based on the general $SEIR$ formulation without vital dynamics.

We divide the population into five classes: susceptible (S), latent (L), pre-symptomatic (P), infected (I), and removed (R). Susceptibles are those who can get infected by SARS-CoV-2. The members of the latent compartment L have already been infected, but are not yet infectious nor do they display any symptoms. After that, latent individuals move to the pre-symptomatic class P meaning that, due to the increased viral load, they are able to infect susceptible individuals, even though, they still not display any symptoms. The existence of pre-symptomatic transmission is of particular importance in analyzing COVID-19 as it is one of the key features of the disease that makes controlling the outbreak difficult. Then, in our model, after the incubation period, at disease onset, members of P move to the infected class I. We note that another challenge with COVID-19 is that many patients will develop mild symptoms or none at all, yet being infectious. It is thus customary to collect these individuals in a separate compartment of asymptomatic individuals [9, 10]. Nevertheless, this distinction is not needed in our model as we will explain later in this section. Finally, patients transit to the removed compartment R by either recovery or by isolation after testing positive for COVID-19.

The above considerations are formulated in the following system of ordinary differential equations

$$\begin{aligned} S'(t) &= -\beta \frac{S(t)}{N(t)} \left(P(t) + I(t)\right), \\ L'(t) &= \beta \frac{S(t)}{N(t)} \left(P(t) + I(t)\right) - \alpha L(t), \\ P'(t) &= \alpha L(t) - \rho P(t), \\ I'(t) &= \rho P(t) - \gamma I(t) - k \frac{pI(t)}{pI(t) + \sigma}, \\ R'(t) &= \gamma I(t) + k \frac{pI(t)}{pI(t) + \sigma}. \end{aligned} \tag{5.1}$$

The disease transmission rate is denoted by the parameter β, the *incubation period* is $\alpha^{-1} + \rho^{-1}$, which is the sum of the duration of the latent period and the *pre-symptomatic* period, and, finally, γ^{-1} stands for the symptomatic infectious period. The transmission diagram of (5.1) is depicted on Fig. 5.1.

The *force of infection* is the rate associated with the outward flow from S to L, namely,

$$\lambda = \beta \frac{1}{N}(P + I).$$

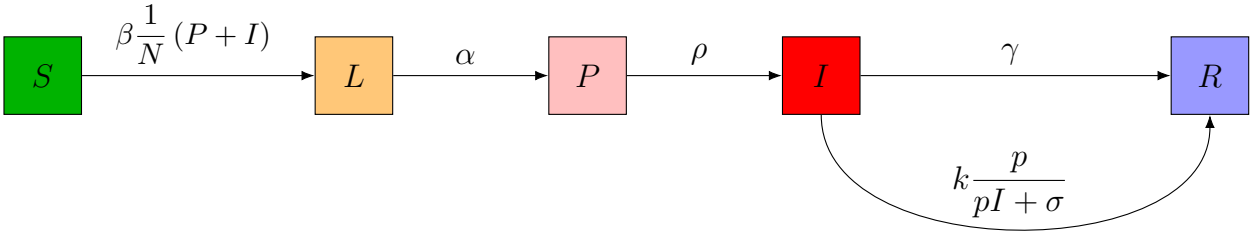

Figure 5.1: The transmission diagram of the $SLPIR$ model (5.1). Arrows represent the transition rates between the compartments.

The indicator symptom-based testing is represented by the term

$$k\frac{pI}{pI+\sigma},$$

where k gives the number of tests done per unit time also referred to as the *testing rate*, the probability p describes how likely is that a member of compartment I displays the chosen indicator symptom. Note that this probability removes the need for an asymptomatic/mild compartment as it is straightforward to adjust p to account for all COVID-19 patients. The final term σ (possibly time-dependent) represents those individuals who are not infected by COVID-19, yet they show the very same symptom we base our testing upon. In this chapter, we refer to σ as the *secondary symptom pool*, whereas, the *primary symptom pool* Σ is composed of all members (with or without COVID-19 infection) of the population displaying the indicator symptom at a given time, that is

$$\Sigma = pI + \sigma.$$

The testing rate k has a natural upper bound, namely,

$$k \leq \Sigma$$

as we solely test patients displaying the indicator symptom. By reformulating the testing term as

$$k\frac{pI}{pI+\sigma} = \frac{k}{\Sigma}\cdot p \cdot I,$$

it is interpreted as the removal of the $\frac{k}{\Sigma}$ fraction of COVID-19 patients displaying the indicator symptom.

The rate of the testing-induced outward flow from I to R is referred to as the *force of testing* given by

$$\tau_{k,p,\sigma} = k\frac{p}{pI+\sigma}. \tag{5.2}$$

Finally, we introduce the *positivity rate* of testing as

$$\theta = \frac{pI}{pI+\sigma}, \tag{5.3}$$

that may serve as a real-time indicator of the severity of an ongoing epidemic, and the adequateness of the testing rate.

Note that (5.1) is, in part, simpler than many other variants that have been used to assess the spread of COVID-19 as the infectious and latent compartments are not split into multiple stages [4, 9, 10, 13, 14]. However, these additional classes carry little significance for the testing strategies and to the analysis presented in this chapter. Hence, we chose to use this less complicated structure so that the emphasis is put on the testing itself.

We have parametrized (5.1) following [6]. From the infectivity profile of COVID-19 [65, 66, 67], we can see that most transmissions occur between 3 days prior to and 4 days after symptom onset, with the pre-symptomatic infection fraction being 43.7%. Thus, it is a reasonable approximation to set the pre-symptomatic period ρ^{-1} as 3 days, and the symptomatic infectious period γ^{-1} as 4 days, with the same infectiousness β during this period. The estimated mean incubation period of COVID-19 is 5.5 days [15], thus, the latent period α^{-1} is taken as 2.5 days, see Table 5.1. The choice of the transmission rate β is discussed in Sect. 5.2.1 and the testing parameters k, p, σ are varied throughout the analysis.

Table 5.1: Parameters of the $SLPIR$ model

Parameter	Notation	Value
Transmission rate	β	Sect. 5.2.1.
Latent period	α^{-1}	2.5 days
Pre-symptomatic (infectious) period	ρ^{-1}	3 days
Infectious period	γ^{-1}	4 days
Testing rate	k	varies
Secondary symptom pool	σ	varies
Probability of symptom amongst COVID-19 patients	p	varies

5.2.1 Choosing the transmission rate β

Now, we concentrate on establishing the relationship between the transmission rate β in (5.1) and the basic reproduction number $\mathcal{R}_0$ of the epidemic. We shall follow the terminology and techniques of [16] to compute the Next Generation Matrix (NGM) and the $\mathcal{R}_0$ as its spectral radius.

First, let us consider the infectious subsystem of (5.1), namely, equations describing $L(t)$, $P(t)$, and $I(t)$. Linearizing this subsystem w.r.t. the disease free equilibrium yields the linearized infectious subsystem

$$X'(t) = (\mathbf{F} - \mathbf{V}) \cdot X(t),$$

where the matrices $\mathbf{F}$ and $\mathbf{V}$ are the Jacobians of the transmission and the transitional part, respectively:

$$\mathbf{F} = \left[\frac{\partial \mathcal{F}_i}{\partial I_j}(DFE)\right], \ \mathbf{V} = \left[\frac{\partial \mathcal{V}_i}{\partial I_j}(DFE)\right].$$

the state is described by

$$X(t) = \begin{bmatrix} L(t) \\ P(t) \\ I(t) \end{bmatrix}.$$

The transmission matrix $\mathbf{F}$ has the form

$$\mathbf{F} = \begin{bmatrix} 0 & \beta & \beta \\ 0 & 0 & 0 \\ 0 & 0 & 0 \end{bmatrix},$$

and the transitional matrix $\mathbf{V}$ is, clearly, written as

$$\mathbf{V} = \begin{bmatrix} -\alpha & 0 & 0 \\ \alpha & -\rho & 0 \\ 0 & \rho & -\gamma \end{bmatrix}.$$

The basic reproduction number $\mathcal{R}_0$ is then obtained by computing the spectral radius of $-\mathbf{F}\mathbf{V}^{-1}$ that is

$$\mathcal{R}_0 = \rho(-\mathbf{F}\mathbf{V}^{-1}).$$

Therefore, as

$$-\mathbf{F}\mathbf{V}^{-1} = \begin{bmatrix} \frac{\beta}{\gamma} + \frac{\beta}{\rho} & \frac{\beta}{\gamma} + \frac{\beta}{\rho} & \frac{\beta}{\gamma} \\ 0 & 0 & 0 \\ 0 & 0 & 0 \end{bmatrix},$$

it follows that

$$\mathcal{R}_0 = \beta \left(\frac{1}{\rho} + \frac{1}{\gamma} \right),$$

providing a scheme for computing β. We list the corresponding transmission rates for the sample values of $\mathcal{R}_0$ used for illustrations in Table 5.2.

Table 5.2: The basic reproduction number $\mathcal{R}_0$ and the corresponding transmission rate β

$\mathcal{R}_0$	2.2	1.8	1.3	1.1
β	0.338	0.277	0.2	0.169

The basic reproduction number $\mathcal{R}_0$ is descriptive for the epidemic at the very beginning of an outbreak and in absence of control measures. For simplicity, we use the phrase basic reproduction number even if social distancing is in place, and by control measure in this chapter we mean the testing, the absence of which is modeled by $k = 0$. Similar key characteristics are the *control reproduction number* $\mathcal{R}_c$ and the *effective reproduction number* $\mathcal{R}_t$. The former describes the epidemic incorporating the effect of interventions, in our case indicator symptom-based testing, but still at the beginning of the outbreak. In contrast, the latter is suitable to measure the spread of the disease as the epidemic is progressing. The corresponding formulae may be obtained via analogous computations to those above as

$$\mathcal{R}_c = \beta \left(\frac{1}{\rho} + \frac{1}{\gamma + k\frac{p}{\sigma}} \right) = \beta \left(\frac{1}{\rho} + \frac{\sigma}{\sigma\gamma + kp} \right) \tag{5.4}$$

and

$$\mathcal{R}_t = \beta \frac{S(t)}{N}\left(\frac{1}{\rho} + \frac{1}{\gamma + \tau_{k,p,\sigma}}\right) = \beta \frac{S(t)}{N}\left(\frac{1}{\rho} + \frac{\Sigma}{\Sigma\gamma + kp}\right) = \beta \frac{S(t)}{N}\left(\frac{1}{\rho} + \frac{1}{\gamma + \frac{k}{\Sigma}p}\right).$$

As the testing rate k is bound by the size of the primary symptom pool Σ, it is apparent that both of the above reproduction numbers satisfy

$$\beta\frac{S}{N}\left(\frac{1}{\rho} + \frac{1}{\gamma + p}\right) \leq \mathcal{R}_c, \mathcal{R}_t \leq \mathcal{R}_0. \tag{5.5}$$

5.3 Dependence of key epidemic quantities on the testing strategy

This section analyzes the symptom-based testing strategy with emphasis on how the force of testing and the effective reproduction number are affected by the particular choice of strategy. Repeatedly, we shall utilize the monotonicity of

$$f(x) = \frac{a + x}{b + x}, \qquad x_1 \leq x_2 \Rightarrow f(x_1) \leq f(x_2),$$

where $0 < a \leq b$ and $0 \leq x$.

First, we summarize trivial monotonicity properties of the force of testing $\tau_{k,p,\sigma}$.

Proposition 5.3.1. *Given a fixed state of* (5.1)*, the force of testing* $\tau_{k,p,\sigma}$ *is*

a) monotonically increasing in k*,*

b) monotonically increasing in $\frac{k}{\Sigma}$*.*

In particular, as $\tau_{k,p,\sigma} = \frac{kp}{\Sigma}$, if $\frac{k}{\Sigma} = \text{const}$, then $\tau_{k,p,\sigma} = \text{const}$, *i.e.* the force of testing strongly correlates to what portion of the primary symptom pool is being tested.

As the epidemic is progressing, we may want to maintain the force of testing by increasing the testing rate k that is testing the same portion of individuals displaying the indicator symptom. Clearly, the required adjustment is linear w.r.t. the size of compartment I, thus, the given constant force of testing may be maintained as long as other logistical constraints make increasing the testing rate feasible.

The choice of the indicator symptom that serves as a basis for selecting patients for testing is clearly of importance. Different indicator symptoms typically have different associated probabilities and secondary symptom pools of non-equal sizes. Thus, it is natural to ask what (p, σ) pair is optimal.

Proposition 5.3.2. *The force of testing* $\tau_{k,p,\sigma}$ *is monotonically decreasing in* $\frac{\sigma}{p}$*.*

Proof. Clearly,

$$k\frac{p_1}{p_1 I+\sigma_1}=\tau_{k,p_1,\sigma_1}\leq\tau_{k,p_2,\sigma_2}=k\frac{p_2}{p_2 I+\sigma_2}$$

is equivalent to

$$\frac{1}{I+\frac{\sigma_1}{p_1}}\leq\frac{1}{I+\frac{\sigma_2}{p_2}}$$

that, in turn, simplifies to

$$\frac{\sigma_2}{p_2}\leq\frac{\sigma_1}{p_1}$$

yielding the required result. □

As we have seen, keeping the fraction $\frac{k}{\Sigma}$ constant results in constant force of testing $\tau_{k,p,\sigma}$. The authorities might obtain some data on the size of the primary symptom pool Σ during an outbreak and use this information for adjusting k on-the-go. When planning for a second wave, historical data on the size of the secondary symptom pool σ may give information on the required level of preparedness. Namely, if we know that σ has now a different size compared to the former outbreak, *e.g.* due to a seasonal variation, we may utilize the size difference of the secondary symptom pools as a guidance for the need for testing capacities as follows.

Proposition 5.3.3. *Given a fixed state of* (5.1)*, consider two secondary symptom pools,* $0\leq\sigma_1\leq\sigma_2$ *for the same indicator symptom that appears amongst members of the compartment* I *with probability* p*. Let* k_1 *and* k_2 *be two testing rates corresponding to the testing strategies for* σ_1 *and* σ_2*, respectively. Then,*

$$\frac{k_2}{k_1}=\frac{\sigma_2}{\sigma_1}$$

implies

$$\tau_{k_1,p,\sigma_1}\leq\tau_{k_2,p,\sigma_2}.$$

Proof. As the state is fixed, the two strategies having equal effect corresponds to the equality

$$k_1\frac{p}{pI+\sigma_1}=\tau_{k_1,p,\sigma_1}=\tau_{k_2,p,\sigma_2}=k_2\frac{p}{pI+\sigma_2}$$

that simplifies to

$$\frac{k_2}{k_1}=\frac{pI+\sigma_2}{pI+\sigma_1}.$$

Then, using the aforementioned monotonicity of $f(x)$, we obtain

$$k_2\leq\frac{\sigma_2}{\sigma_1}k_1.$$

Finally, the monotonicity of $\tau_{k,p,\sigma}$ in k completes the proof. □

Recall, that the force of testing $\tau_{k,p,\sigma}$ explicitly appears in the formula for the effective reproduction number $\mathcal{R}_t$ as

$$\mathcal{R}_t = \beta \frac{S}{N} \left(\frac{1}{\rho} + \frac{1}{\gamma + \tau_{k,p,\sigma}} \right).$$

Accordingly, $\mathcal{R}_t$ may be kept decreasing by varying k as discussed in the first half of this section that is by keeping $\tau_{k,p,\sigma}$ constant or increasing. However, in practice, increasing k may eventually become infeasible. At that point, the force of testing will decrease, hence, $\mathcal{R}_t$ may increase temporarily, within the bounds given in (5.5), despite the constantly decreasing number of susceptible individuals $S(t)$.

A reasonable goal for the authorities is to keep $\mathcal{R}_t$ close to a designated value, ideally close to 1 to suppress the epidemic. Running estimates of the actual $\mathcal{R}_t$ might be obtained [10, 18, 19], hence, we investigate if, by an increase of the testing rate, we can alter $\mathcal{R}_t$ as desired.

Proposition 5.3.4. *Let $0 \leq k_1 \leq k_2$ be two testing rates. Consider an epidemic described by (5.1) with daily testing rate k_1, and the associated effective reproduction number $\mathcal{R}_t(k)$ as a function of k.*

Then, the ratio of the effective reproduction numbers corresponding to altering the testing rate from k_1 to k_2

$$r = \frac{\mathcal{R}_t(k_2)}{\mathcal{R}_t(k_1)}$$

satisfies the following inequality

$$\max\left\{ \frac{k_1}{k_2}, \frac{\gamma}{\rho + \gamma} \right\} \leq r \leq 1.$$

Proof. The right bound is trivial as $\mathcal{R}_t$ is monotonic in k. Now, observe that

$$r = \frac{\frac{\Sigma}{k_2 p + \Sigma\gamma} + \frac{1}{\rho}}{\frac{\Sigma}{k_1 p + \Sigma\gamma} + \frac{1}{\rho}}.$$

Then,

$$r = \frac{\frac{\Sigma\rho + \Sigma\gamma + k_2 p}{k_2 p\rho + \Sigma\gamma\rho}}{\frac{\Sigma\rho + \Sigma\gamma + k_1 p}{k_1 p\rho + \Sigma\gamma\rho}} = \frac{\Sigma(\rho+\gamma) + k_2 p}{\Sigma(\rho+\gamma) + k_1 p} \cdot \frac{k_1 p\rho + \Sigma\gamma\rho}{k_2 p\rho + \Sigma\gamma\rho} = \frac{\Sigma(\rho+\gamma) + k_2 p}{\Sigma(\rho+\gamma) + k_1 p} \cdot \frac{k_1 p + \Sigma\gamma}{k_2 p + \Sigma\gamma}.$$

The first term is ≥ 1, thus,

$$r \geq \frac{k_1 p\rho + \Sigma\gamma\rho}{k_2 p\rho + \Sigma\gamma\rho} \geq \frac{k_1 p}{k_2 p} = \frac{k_1}{k_2}$$

using the monotonicity of $f(x)$ noted at the beginning of this section.

Now, consider reordering the product as

$$r = \frac{\Sigma(\rho+\gamma) + k_2 p}{k_2 p + \Sigma\gamma} \cdot \frac{k_1 p + \Sigma\gamma}{\Sigma(\rho+\gamma) + k_1 p}.$$

Again, the first term is ≥ 1, therefore,

$$r \geq \frac{k_1 p + \Sigma\gamma}{\Sigma(\rho+\gamma) + k_1 p} \geq \frac{\Sigma\gamma}{\Sigma(\rho+\gamma)} = \frac{\gamma}{\rho+\gamma}$$

holds using, again, the monotonicity of $f(x)$.

Combining the two inequalities above completes the proof. □

The implications of Prop. 5.3.4 on goals for the testing strategy are rather important as they point out some hard limitations. Clearly, as

$$0.43 \sim \frac{\gamma}{\rho+\gamma},$$

no matter our testing capacity or indicator symptom, we may not suppress the epidemic any further. As an example, if our current estimates for $\mathcal{R}_t$ are above 2.4, then we cannot expect the pure indicator symptom-based testing strategy (without contact-tracing) to be able to suppress the epidemic as $2.4 \cdot 0.43 \sim 1.03$. Additionally, as the indicator symptom limits our testing rate to $k \leq \Sigma = pI + \sigma$, we obtain another hard constraint, namely,

$$r \geq \frac{k_1}{\Sigma}$$

that is the ratio describing what proportion of the primary symptom pool is being tested directly limits the factor which the effective reproduction number may be decreased with via larger testing rates. Finally, we note that reordering the inequality yields $k_2 \geq \frac{k_1}{r}$ as a lower requirement for the required testing rate – given that the reduction by factor r is achievable.

We have discussed from various aspects that increasing the testing rate k decreases the effective reproduction number $\mathcal{R}_t$ that is it has a positive effect on the severity of the epidemic. Nevertheless, this positive effect is gradually decreasing as described by the following Proposition.

Proposition 5.3.5. *Consider the logarithmic derivative of $\mathcal{R}_t$ w.r.t. the testing rate k that is*

$$\mathcal{R}_t^* = \frac{\partial}{\partial k} \log(\mathcal{R}_t).$$

Then, $\mathcal{R}_t^*$ is negative and monotonically increasing in k.

Proof. Clearly,

$$\mathcal{R}_t^* = \frac{\frac{\partial \mathcal{R}_t}{\partial k}}{\mathcal{R}_t} = \frac{-\Sigma\rho p}{(kp+\Sigma\gamma)(kp+\Sigma(\rho+\gamma)} \leq 0.$$

Then,

$$\frac{\partial \mathcal{R}_t^*}{\partial k} = \frac{(\Sigma\rho p)(2kp + \Sigma p(\rho+2\gamma))}{(kp+\Sigma\gamma)^2(kp+\Sigma(\rho+\gamma)^2} \geq 0$$

completes the proof. □

This logarithmic derivative is a measure of the relative change in $\mathcal{R}_t$ w.r.t. the testing rate k. Prop. 5.3.5 states that the relative change is decreasing in absolute value as k increases.

5.4 Numerical simulations

This section presents the results from several numerical simulations demonstrating the impact of the key parameters of the epidemic model (5.1). All simulations were executed with a sample population of size $10,000,000$ with initial conditions placing 1000 individuals into the class L and the rest into S.

First, Sect. 5.4.1 presents the numerical analysis of the control reproduction number $\mathcal{R}_c$. Then, we investigate the connection between the progress of an outbreak and the positivity rate of testing in Sect. 5.4.2. We study the implications of maintaining a constant force of testing $\tau_{p,k,\sigma}$ in Sect. 5.4.3. The significance of the seasonality of the secondary symptom pool σ is analyzed in Sect. 5.4.4. Finally, in Sect. 5.4.5, we assess how an increased testing rate may delay the progress of COVID-19.

5.4.1 The effect of testing on the control reproduction number $\mathcal{R}_c$

The control reproduction number $\mathcal{R}_c$, given in (5.4), describes the initial progress of the epidemic at its very beginning. Fig. 5.2 demonstrates what effect of indicator symptom-based testing has on $\mathcal{R}_c$ for various values of $\mathcal{R}_0$ and σ.

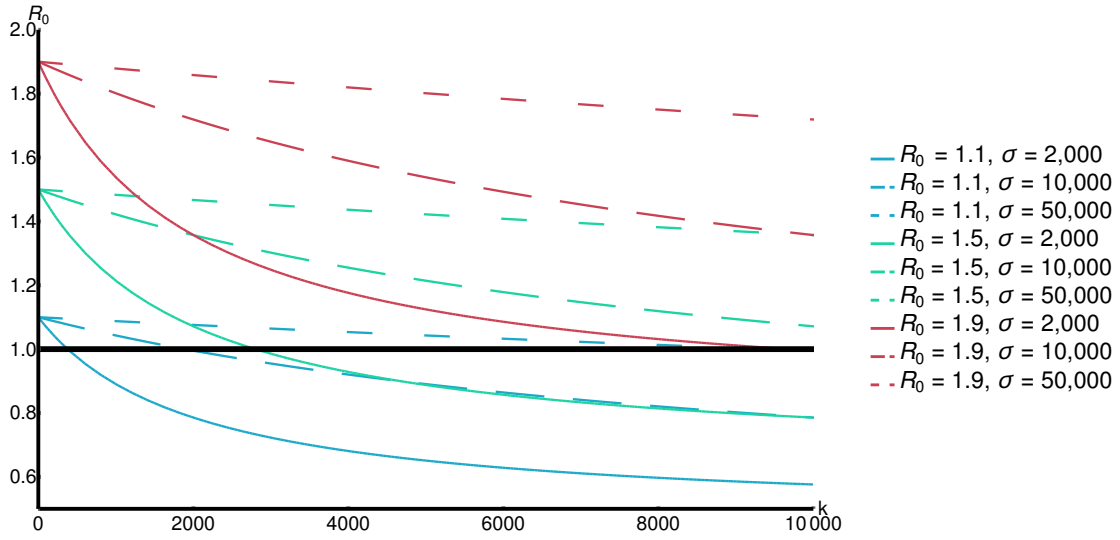

Figure 5.2: The effect of indicator symptom-based testing on $\mathcal{R}_c$ for $p = 0.25$.

Clearly, larger maximal testing rate k results in lower $\mathcal{R}_c$. The size of the secondary symptom pool σ apparently greatly affects the decrease we may achieve by larger k.

5.4.2 The progress of an outbreak and the positivity rate θ

Recall that the positivity rate θ, see (5.3), is a key feature of the testing strategy that may be readily observed during an outbreak. If the efforts aimed at suppressing COVID-19 are not successful, the rate θ will increase as the term $pI(t)$ will eventually dominate the secondary symptom pool σ. Fig. 5.3 demonstrates that the changes in θ are in close connection with

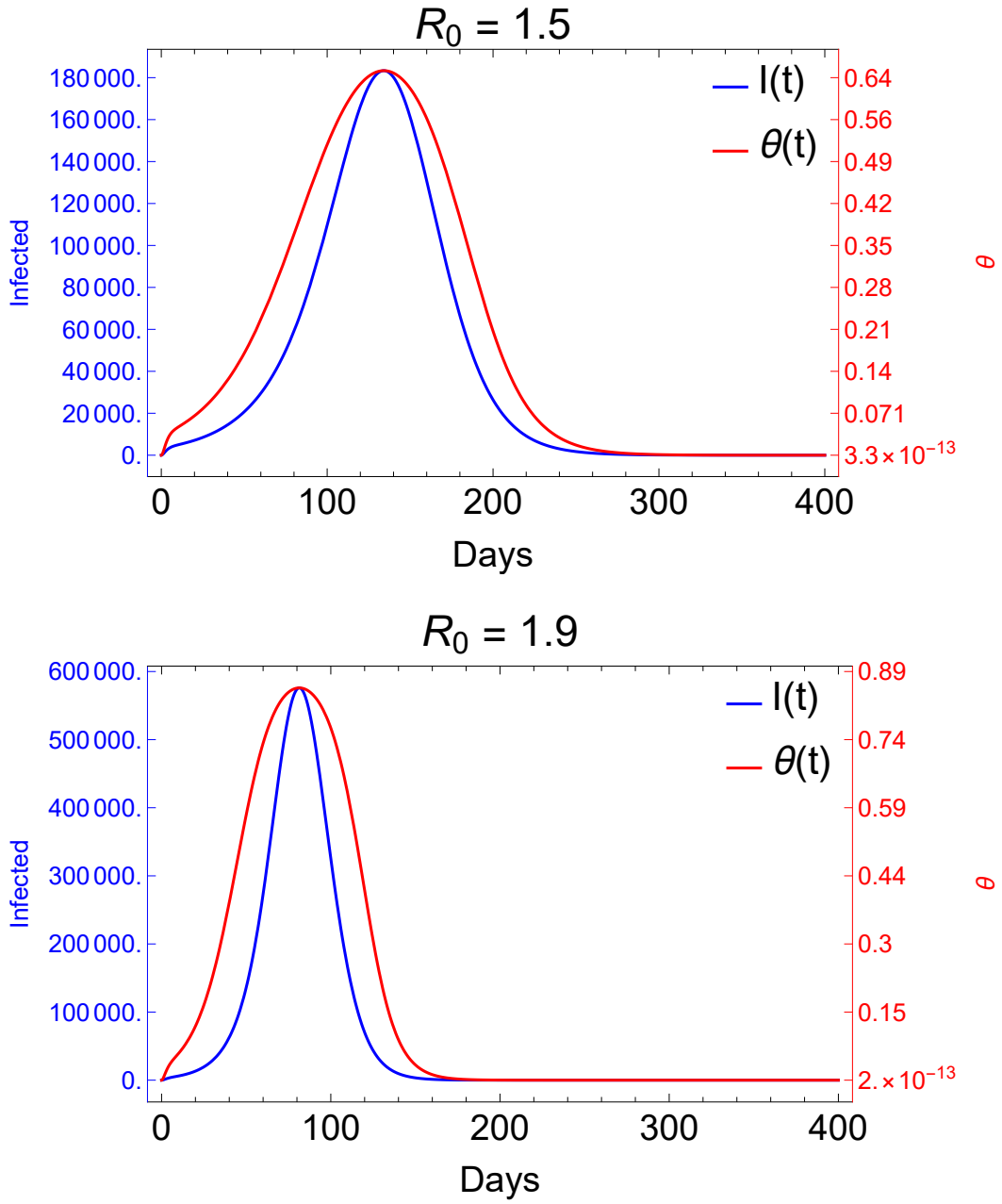

Figure 5.3: Evolution of the positivity rate during outbreaks of different magnitudes. The prevalence of the indicator symptom is $p = 0.1$ with a maximal testing capacity $k = 10{,}000$ and secondary symptom pool $\sigma = 10{,}000$.

the dynamics of $I(t)$. This relationship between θ and $I(t)$ carries a certain benefit for the authorities as the increase of the positivity rate precedes that of the epidemic curve, hence, it may serve as a primary indicator for the progress of an epidemic.

5.4.3 Implications of constant force of testing $\tau_{p,k,\sigma}$

As we have discussed in Sect. 5.3, a constant force of testing $\tau_{p,k,\sigma}$ is achieved by testing a fixed portion of the primary symptom pool Σ, *i.e.* $\frac{k}{\Sigma}$ is constant. For an ongoing epidemic this results in a constant increase in the required daily testing rate k. We have analyzed the maximal required testing capacity w.r.t. COVID-19 patients in Fig. 5.4.

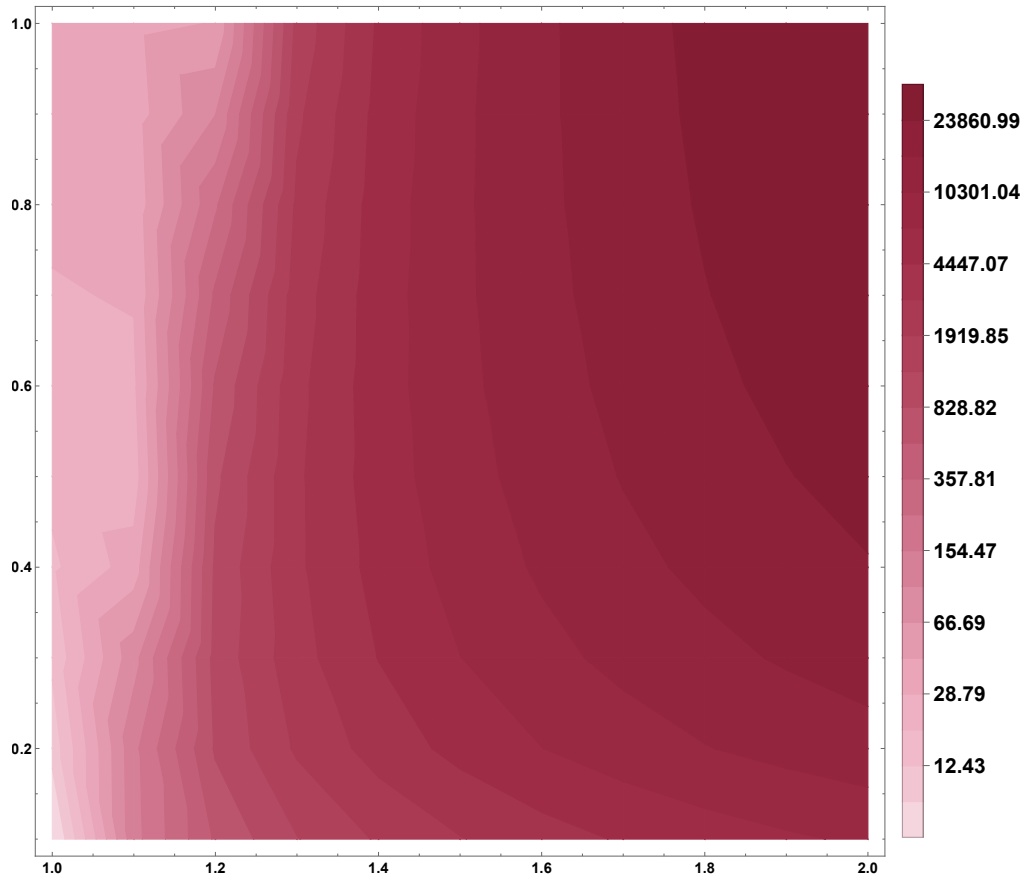

Figure 5.4: Required testing capacity to maintain a constant force of testing $\tau_{p,k,\sigma}$. The vertical axis describes the desired portion for testing the primary symptom pool and the horizontal axis represents the underlying basic reproduction number $\mathcal{R}_0$. The prevalence of the indicator symptom is set to $p = 0.1$.

Note that for constant $\tau_{p,k,\sigma}$, the system (5.1) is independent of the secondary symptom pool σ, thus, this requirement must be adjusted based on historical data on the size of σ to obtain the total maximal required capacity.

5.4.4 Seasonality of the secondary symptom pool σ

Now, let us investigate the epidemic curves in case of a periodically varying secondary symptom pool. To that end, we employ a commonly used seasonality function

$$\omega(t) = 365 \cdot \frac{10^{b\cos\left(\frac{2\pi(t-c)}{365}\right)}}{\int_0^{365} 10^{b\cos\left(\frac{2\pi(t-c)}{365}\right)} dt},$$

with $b = 0.5$ and consider $\sigma = \sigma_{\text{avg}} \cdot \omega(t)$. The parameter c is used to model shift in

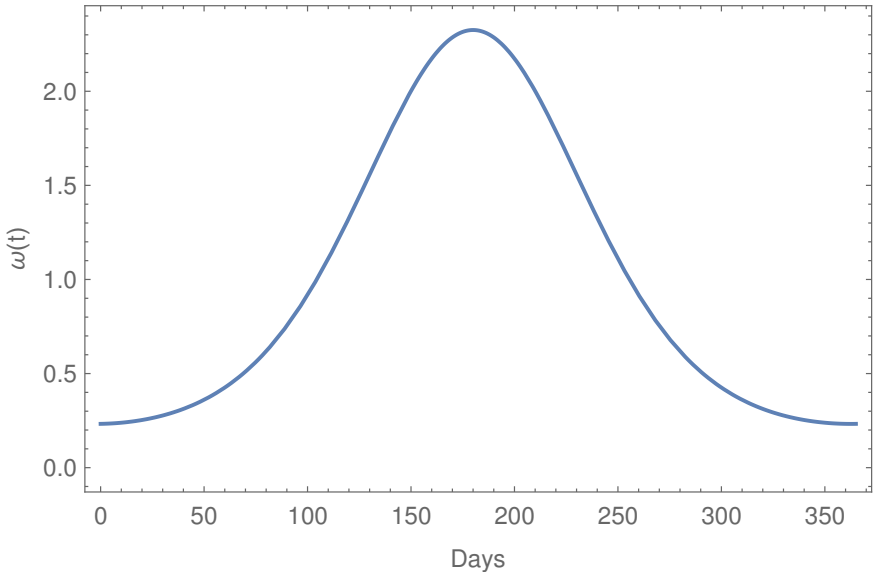

Figure 5.5: The seasonality function $\omega(t)$ with $c = 183$. This corresponds to minimal secondary symptom pool at the beginning of an outbreak.

the seasonality, *i.e.* to analyze the differences between an outbreak starting at minimal or maximal secondary symptom pools. The function $\omega(t)$ is displayed on Fig. 5.5 for the case of minimal secondary symptom pool at time $t = 0$ that is for a shift $c = 183$.

Fig. 5.6 demonstrates the effect of having seasonality in σ and the COVID-19 outbreak beginning around the minimal size of the secondary symptom pool. This comparison shows that we may expect a slight, but notable, delay in this scenario compared to the non-seasonal setting.

5.4.5 The effect of varying the testing rate k

Increasing the testing rate k has a beneficial effect. We demonstrate this via transitional plots on Fig. 5.7. Note that a larger maximal k both delays in time and decreases in size the peak of the epidemic.

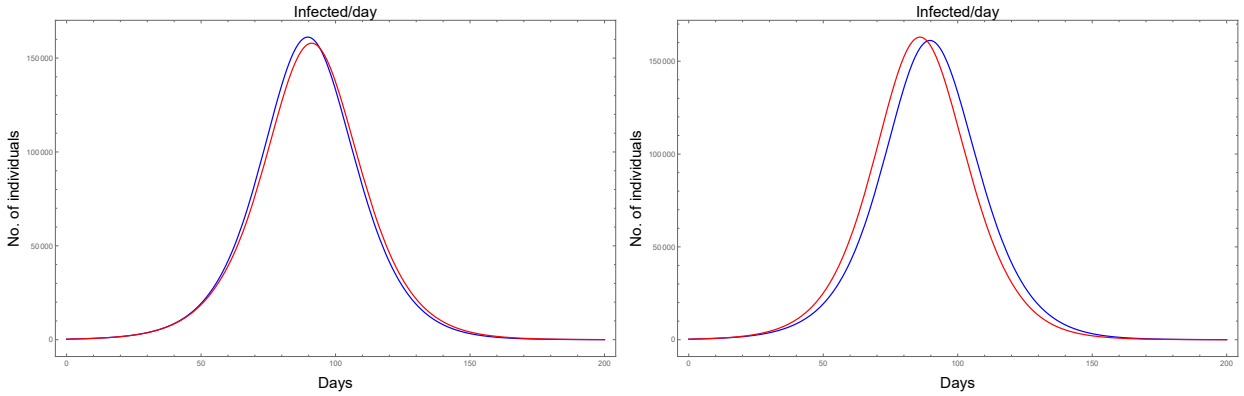

Figure 5.6: The impact of seasonal σ with minimal (left) and maximal (right) size at the beginning of the outbreak. $\mathcal{R}_0 = 1.9$, $p = 0.1$, $k = 10{,}000$, $\sigma = 10{,}000$. The blue curve corresponds to assuming a constant (average) secondary symptom pool, whilst, the red curve depicts the effect of seasonality.

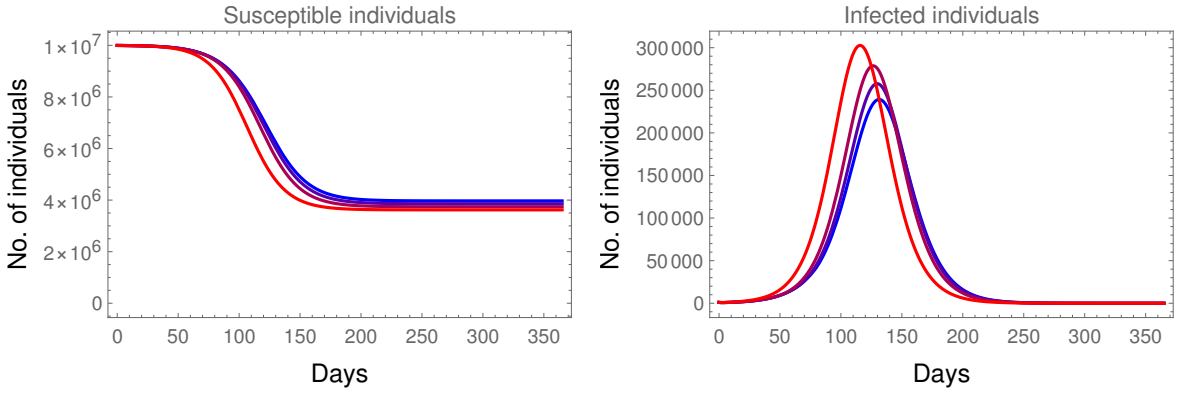

Figure 5.7: The impact of increasing the testing rate from 1,000 (red) to 10,000 (blue) using parameters $\mathcal{R}_0 = 1.6$, $p = 0.1$, $1,000 \leq k \leq 10{,}000$, $\sigma = 10{,}000$.

6

Adaptive group testing in a compartmental model of COVID-19

6.1 Transmission models with pooling

In this section, we develop a compartmental model to describe mass testing along with the application of various pooling methods and confinement of those tested positively. The population is divided into five classes: susceptibles, latent, presymptomatic, infected and removed, denoted by S, L, P, I and R, respectively. Susceptibles are those who can be infected by coronavirus, latent are those who have been infected, but do not show symptoms, and neither can transmit the disease. Presymptomatic individuals still do not show symptoms but they can infect others as well. Latent individuals move to the infected class after a latency period, while following recovery, people from the infected class proceed to the removed compartment. In this model, we ignore any disease-induced death and demography. This *SLPIR* model is further developed by considering the effects of mass testing in our equations, i.e., we include terms for removing individuals whose test evaluated positively (from any of the five classes). In the following, compartment $Q(t)$ will stand for the temporarily confined at time t, and we assume an active quarantine, in which the population compensates the loss of links rewiring the ineffective connections towards nonquarantining nodes [63]. After an isolation of τ days, the quarantined individuals move back into the S or R class, depending on the status of a given individual. We introduce the notation $N(t) = S(t) + L(t) + P(t) + I(t) + R(t)$ for the total active population, i.e. for those who are not in confinement. We note that, as we mentioned before, the total population $S(t) + L(t) + P(t) + I(t) + R(t) + Q(t) = \Pi$ is constant.

Removal of positively tested individuals and putting back those who have passed τ days in confinement are both considered in various ways in the equations, modeling different methods applied in mass testing. Namely, we consider two different pooling methods.

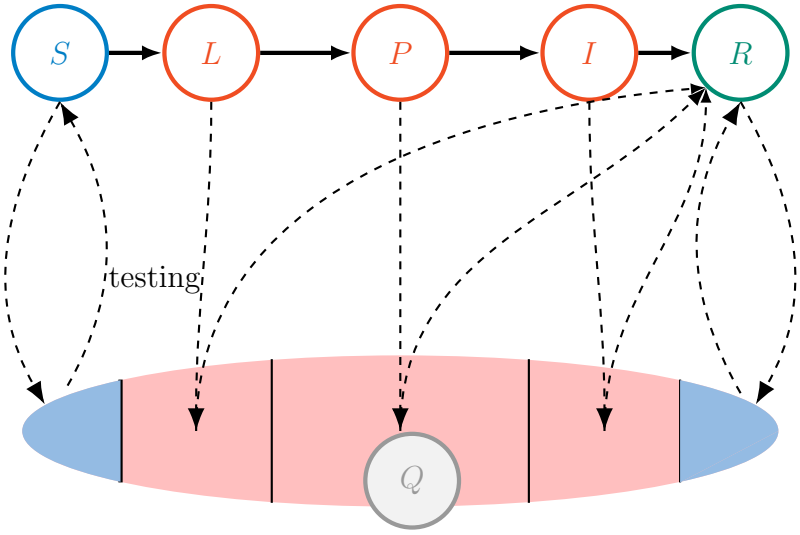

Figure 6.1: Transmission diagram for the *SLPIR* model with quarantine.

6.2 Regular pooling

In the case of regular pooling, we select k individuals and perform a single RT-PCR test on their combined (pooled) samples. Even if the test comes back as positive, no additional tests are performed to identify the infected individuals, instead of that, everybody in the pool will be confined. We apply the notation p for the sensitivity of the test, i.e. the probability that a test gives a correct positive result when the sample contains viral particles. In general, the sensitivity of the tests may depend on several factors, for example the brand of the test, whether the tested individual was symptomatic or asymptomatic, the number of days elapsed since exposure, in the case of pooling the size and the composition of the pool. For simplicity, here we assume an average sensitivity value $p = 0.9$, which is in line with [50, 61], and use this value throughout the chapter. We denote by $1-\rho$ the specificity of the test, i.e. ρ is the probability of the test giving a false positive result in case of a non-infected person being tested. In the following, σ stands for the number of people tested each day. With this approach, we determine the number of individuals removed from each compartment on a given day. We note that the sensitivity and specificity of testing a pool of several samples might differ from those of an individual test as it might depend on the number of positive samples included in the pool. However, for the sake of simplicity, we will ignore this difference in this chapter.

The number of individuals isolated from the L, P or I compartments is given by the number of individuals from these compartments being tested multiplied by the sensitivity, i.e. $\sigma \cdot \frac{L(t)}{N(t)} \cdot p$, $\sigma \cdot \frac{P(t)}{N(t)} \cdot p$ and $\sigma \cdot \frac{I(t)}{N(t)} \cdot p$, respectively.

The number of individuals isolated from the S or R compartments can be obtained by the following. Assume someone is in a positive pool. Considering the other $k-1$ individuals in the same pool,

1. either there is an individual who is in compartment L, P or I and the pool is true positive,

2. or everyone else is from the S or R compartment as well, and the pool is false positive.

Therefore we obtain that the expected number of individuals being isolated from the S or R compartment can be obtained as

$$\sigma \cdot \tfrac{S(t)}{N(t)} \cdot U(t) \text{ and } \sigma \cdot \tfrac{R(t)}{N(t)} \cdot U(t), \text{ respectively,}$$

where

$$\begin{aligned} U(t) &= \left[1 - \left(\tfrac{S(t)+R(t)}{N(t)}\right)^{k-1}\right] \cdot p + \left(\tfrac{S(t)+R(t)}{N(t)}\right)^{k-1} \cdot \rho \\ &= \left[1 - (1-\pi(t))^{k-1}\right] \cdot p + (1-\pi(t))^{k-1} \cdot \rho, \end{aligned}$$

where $\pi(t) = \frac{L(t)+P(t)+I(t)}{N(t)}$ stands for the disease prevalence. The delay differential equation system describing the dynamics (we start to test individuals at $t = 0$) can be written as

$$\begin{aligned} S'(t) = & -\beta \frac{S(t)}{N(t)} (I(t) + P(t)) - \sigma \cdot \frac{S(t)}{N(t)} \cdot U(t) \\ & + \sigma \cdot \frac{S(t-\tau)}{N(t-\tau)} \cdot U(t-\tau) \cdot H(t-\tau), \\ L'(t) = & \beta \frac{S(t)}{N(t)} (I(t) + P(t)) - \alpha_{_L} L(t) - p\sigma \frac{L(t)}{N(t)}, \\ P'(t) = & \alpha_{_L} L(t) - \alpha_{_P} P(t) - p\sigma \frac{P(t)}{N(t)}, \\ I'(t) = & \alpha_{_P} P(t) - \gamma I(t) - p\sigma \frac{I(t)}{N(t)}, \\ R'(t) = & \gamma I(t) - U(t)\sigma \frac{R(t)}{N(t)} \\ & + H(t-\tau) p\sigma \frac{L(t-\tau) + P(t-\tau) + I(t-\tau)}{N(t-\tau)} \\ & + H(t-\tau) \cdot U(t-\tau)\sigma \frac{R(t-\tau)}{N(t-\tau)}, \end{aligned} \tag{6.1}$$

where

$$H(t-\tau) = \begin{cases} 0, & t < \tau, \\ 1, & t \geq \tau \end{cases}$$

is the Heaviside step function. The parameter β is used for disease transmission rate, $\alpha_{_L}^{-1}$ denotes the average length of the latent period, $\alpha_{_P}^{-1}$ stands for the average time from becoming infectious until symptoms onset, while γ denotes recovery rate.

The above mentioned compartment $Q(t)$ is aggregated as

$$\begin{aligned} Q'(t) = & U(t) \cdot \sigma \frac{S(t) + R(t)}{N(t)} - H(t-\tau) U(t-\tau) \sigma \frac{S(t-\tau) + R(t-\tau)}{N(t-\tau)} \\ & + p\sigma \frac{L(t) + P(t) + I(t)}{N(t)} - H(t-\tau) p\sigma \frac{L(t-\tau) + P(t-\tau) + I(t-\tau)}{N(t-\tau)}. \end{aligned}$$

Let us note that the quarantine compartment does not appear in any of the equations of (6.1), hence, it can be studied independently from the equation of $Q(t)$.

System (6.1) is an *SLPIR*-type disease model assuming exponentially distributed latent, presymptomatic and infectious period. The basic reproduction number of the model without mass testing (i.e. for $\sigma = 0$), considering infectiousness for compartments P and I is given by

$$R_0 = \beta \cdot \left(\alpha_P^{-1} + \gamma^{-1}\right).$$

We assume that infected individuals are removed from compartments L, P and I with rate $p\sigma$ and put back to the compartments τ days later. We catch the latter event in the system using terms with time-delay. Therefore, introducing the notation $\hat{\sigma} = \frac{\sigma}{\Pi}$ for the fraction of the population tested each day, and tracking the progress of a single infected individual through the infected compartments, we get the control reproduction number as

$$\begin{aligned} R_{c,\text{mass}} &= \frac{\alpha_L}{\alpha_L + p\hat{\sigma}} \cdot \frac{\beta}{\alpha_P + p\hat{\sigma}} + \frac{\alpha_L}{\alpha_L + p\hat{\sigma}} \cdot \frac{\alpha_P}{\alpha_P + p\hat{\sigma}} \cdot \frac{\beta}{\gamma + p\hat{\sigma}} \\ &= \frac{\alpha_L \beta(\alpha_P + \gamma + p\hat{\sigma})}{(\alpha_L + p\hat{\sigma})(\alpha_P + p\hat{\sigma})(\gamma + p\hat{\sigma})}. \end{aligned}$$

The parameters and their values used in our simulations are shown in Table 6.1. The model is parametrized by values from various studies in the literature [58, 59, 60, 61, 62].

Parameter	**Interpretation**	**Value (range)**	**Reference**
R_0	Basic reproduction number	varies	[58]
α_L^{-1}	Latent period	2.5 (days)	[59]
α_P^{-1}	Presymptomatic period	3 (days)	[59]
γ^{-1}	Infectious period	4 (days)	[59]
β	Transmission rate	varies	calculated from R_0
$1-\rho$	Specificity	0.98 (0.9–1)	[60]
p	Sensitivity	0.9 (0.62–0.98)	[50, 61, 62]
Π	Population size	$10,000,000$	-
σ	Number of individuals tested each day	$[0, \Pi]$	-
k	Number of samples in a pool	1–32	[50]
τ	Duration of quarantine	14 days	[57]

Table 6.1: Parameters and values applied in simulations.

6.2.1 Numerical results for regular pooling

In this subsection, we present the effect of regular pooling on the epidemic curves of the infected and quarantined. Below we compare six different scenarios: a simple mass testing method with 1% of the population tested daily, and five cases of regular pooling with pool sizes of 5, and 1–5% of the population being tested daily. Figure 6.2 shows a comparison of

these scenarios, suggesting that with the same amount of tests performed, pooling can be much more effective for mitigating the epidemic. However, regular pooling with a large pool size will increase the number of quarantined people to such an extent which is impossible to be realized in real life.

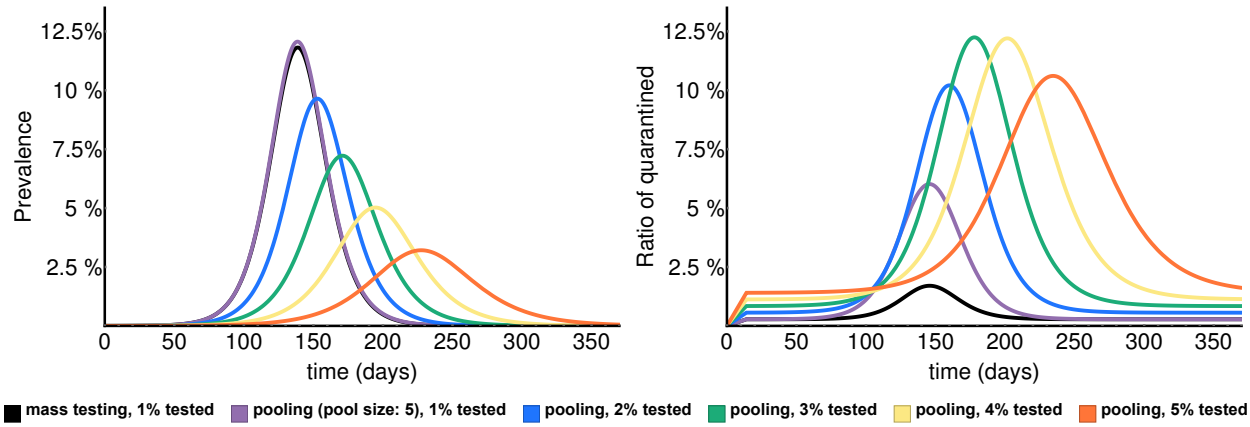

Figure 6.2: Epidemic curves with different pooling methods with parameters taken from Table 6.1, and $R_c = 1.8$. The black curves represent the regular mass testing method with 1% of the population being tested each day. It is worth mentioning that we need the same number of tests for the strategies leading to the black and the orange curve.

6.2.2 Dorfman pooling

In the case of Dorfman pooling, we select k individuals and perform a single *RT-PCR* test on their combined (pooled) samples. If the pooled test yields a positive result, then each sample is retested separately and we only remove those individuals who were retested as positive; otherwise, everyone is declared negative. We note that there are other, more intricate methods for arranging the pools [64].

We determine the number of individuals removed from each compartment on a given day. If this person is from compartment L, P or I, then we obtain the expected number of individuals being isolated from these compartments by multiplying the number of latent, presymptomatic or infected people being tested with two probabilities: that of the pool comes back as positive and that of the individual test gives a correct positive result.

This product gives us $\sigma\frac{L(t)}{N(t)} \cdot p^2$, $\sigma\frac{P(t)}{N(t)} \cdot p^2$, and $\sigma\frac{I(t)}{N(t)} \cdot p^2$, respectively.

The number of individuals isolated from the S or R compartments can be obtained by the following. Assume that a non-infected is in a positive pool. Considering the other $k-1$ individuals in the same pool,

1. either there is an individual who is in compartment L, P or I, the pool is true positive and the individual test is a false positive;

2. or everyone else is from the S or R compartment as well, the pool is false positive and the individual test is false positive result as well.

Therefore we obtain that the expected number of individuals being isolated from the S or R compartment can be obtained as

$$\sigma \cdot \tfrac{S(t)}{N(t)} \cdot U(t) \text{ and } \sigma \cdot \tfrac{R(t)}{N(t)} \cdot U(t), \text{ respectively,}$$

where

$$U(t) = \left(\left[1 - \left(\tfrac{S(t)+R(t)}{N(t)} \right)^{k-1} \right] \cdot p \cdot \rho + \left(\tfrac{S(t)+R(t)}{N(t)} \right)^{k-1} \cdot \rho^2 \right).$$

The system describing the dynamics can be written as

$$\begin{aligned}
S'(t) =& -\beta \frac{S(t)}{N(t)} \left(I(t) + P(t)\right) - U(t) \cdot \sigma \frac{S(t)}{N(t)} + H(t-\tau)U(t-\tau)\sigma \frac{S(t-\tau)}{N(t-\tau)}, \\
L'(t) =& \beta \frac{S(t)}{N(t)} \left(I(t) + P(t)\right) - \alpha_{_L} L(t) - p^2 \sigma \frac{L(t)}{N(t)}, \\
P'(t) =& \alpha_{_L} L(t) - \alpha_{_P} P(t) - p^2 \sigma \frac{P(t)}{N(t)}, \\
I'(t) =& \alpha_{_P} P(t) - \gamma I(t) - p^2 \sigma \frac{I(t)}{N(t)}, \\
R'(t) =& \gamma I(t) - U(t)\sigma \frac{R(t)}{N(t)} + H(t-\tau)p^2\sigma \frac{L(t-\tau) + P(t-\tau) + I(t-\tau)}{N(t-\tau)} \\
&+ H(t-\tau) \cdot U(t-\tau)\sigma \frac{R(t-\tau)}{N(t-\tau)},
\end{aligned} \tag{6.2}$$

with the equation for the quarantine compartment $Q(t)$ obtained as

$$\begin{aligned}
Q'(t) = U(t) \cdot \sigma \frac{S(t) + R(t)}{N(t)} - H(t-\tau)U(t-\tau)\sigma \frac{S(t-\tau) + R(t-\tau)}{N(t-\tau)} \\
+ p^2 \sigma \frac{L(t) + P(t) + I(t)}{N(t)} - H(t-\tau)p^2\sigma \frac{L(t-\tau) + P(t-\tau) + I(t-\tau)}{N(t-\tau)}.
\end{aligned}$$

The control reproduction number of the model with pooling using follow-up can be calculated as

$$R_{c,\text{pool-with-follow-up}} = \frac{\alpha_{_L}}{\alpha_{_L} + p^2\hat{\sigma}} \cdot \frac{\beta}{\alpha_{_P} + p^2\hat{\sigma}} + \frac{\alpha_{_L}}{\alpha_{_L} + p^2\hat{\sigma}} \cdot \frac{\alpha_{_P}}{\alpha_{_P} + p^2\hat{\sigma}} \cdot \frac{\beta}{\gamma + p^2\hat{\sigma}}.$$

6.2.3 Comparison of regular and Dorfman pooling

In this subsection, we compare the effect on the epidemic curves of the infected and quarantined applying regular and Dorfman pooling.

Figure 6.3 shows a comparison of these scenarios, suggesting that with Dorfman pooling, the number of infected slightly increases. An explanation to this is that individuals from the infectious compartments need to give an additional true-positive test in order to get confined. The most important effect of the followup measure shows on the number of quarantined. This is caused by the fact that the number of individuals getting quarantined from non-infected compartments decreases substantially.

Using Dorfman pooling has another important advantage. Considering a situation after the outbreak diminishes, susceptible or removed individuals will get confined because of

the false-positive tests. With regular pooling, one false-positive test is enough to become isolated, that is,

$$\lim_{t\to\infty} Q(t) = \sigma \cdot \rho \cdot \tau,$$

while, with Dorfman pooling,

$$\lim_{t\to\infty} Q(t) = \sigma \cdot \rho^2 \cdot \tau.$$

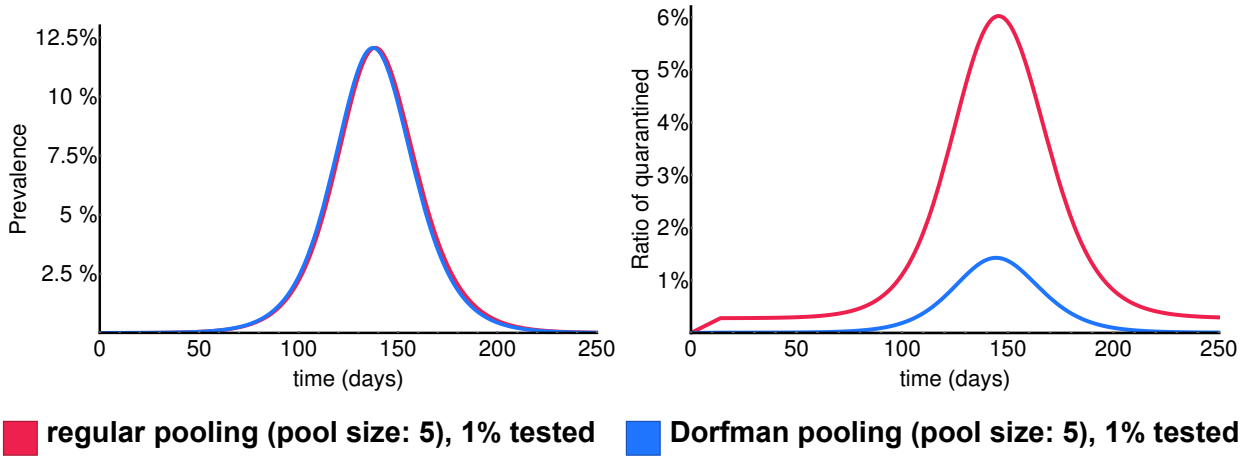

Figure 6.3: Comparison of regular and Dorfman pooling in terms of the infected and quarantined. Parameters p and ρ are taken from Table 6.1, $R_c = 2.5$.

We have to consider, though, that in (6.2), considering Dorfman pooling, if we test the same number of individuals, we require significantly more tests because of those we use for the individual tests. In Section 6.3, we investigate this issue rigorously.

6.3 Optimization of Dorfman pooling

As we mentioned, Dorfman pooling is more feasible in terms of the number of isolated people, but on the other hand, it requires higher testing capacity. It is straightforward that as the prevalence increases, the probability of a positive pool increases as well, therefore we need more tests and fewer people can be removed from the epidemic chain. Note that, in general, testing capacities are limited, usually there is a certain number of tests which can be evaluated in a day. In the following, let us denote the number of tests available for one day by $\mathcal{T}$. We consider a feasible range of prevalence π varying during the course of the outbreak as $0 \leq \pi \leq 0.1$.

Thus, we can derive

$$\begin{aligned}\mathcal{T} &= \#\{\text{pools}\} + k \cdot \#\{\text{positive pools}\} \\ &= \frac{\sigma}{k} + k \cdot \frac{\sigma}{k} \cdot P(\text{a pool is positive}) \\ &= \frac{\sigma}{k} + \sigma \cdot \left(\left(1 - (1-\pi)^k\right) \cdot p + (1-\pi)^k \cdot \rho\right).\end{aligned}$$

Which yields

$$\sigma = \frac{\mathcal{T}}{\frac{1}{k} + P\,(\text{a pool is positive})} = \frac{\mathcal{T}}{\frac{1}{k} + \left(1 - \left(1-\pi\right)^k\right) \cdot p + \left(1-\pi\right)^k \cdot \rho}. \tag{6.3}$$

We would like to emphasize that the prevalence is changing according to the disease dynamics, therefore, σ is changing in time as well.

6.4 Finding $\mathcal{T}$ for a fixed pool size

Now we can determine the maximal number of tests which could be necessary for obtaining the blue curve on Figure 6.2. Using the parameters from Table 6.1 for p and ρ, with basic calculus we can obtain that the maximum of the denominator in (6.3) is obtained at $\pi = 0.1$ indeed, and it is

$$100,000 \cdot \left(\frac{1}{5} + \left(1 - \left(1-0.1\right)^5\right) \cdot 0.9 + \left(1-0.1\right)^5 \cdot 0.02\right) \approx 58,037$$

However, we only need $100,000/5 = 20,000$ tests per day for obtaining the red (regular pooling) curve.

6.4.1 Optimizing the pool size depending on prevalence

An important question regarding pooling is to determine the optimal pool size. Large pool size enable to test several samples at the same time, however, a large sample size can lead to inaccuracies and also increases the probability of the presence of a positive sample. This, in turn implies that all samples in that pool have to be tested again. Hence, if prevalence is high, then large pool sizes might make nullify the benefits of pooling. On the other hand, if prevalence is low, larger pool sizes seem to be the better choice as there is a larger probability of samples being negative.

To complete all the necessary follow-up tests, we need to allocate a fraction of available tests. Next we determine the minimal quantity required for this purpose, which are sufficient for any possible prevalence.

We would like to determine the worst case scenario, namely, the minimal value of $\sigma(t)$ with our restrictions. We can always confine that many individuals, regardless of the prevalence.

In other words, we are looking for the maximum of the denominator in (6.3).

To determine the optimal pool size k in order to maximize the denominator in (6.3), we differentiate

$$\frac{1}{k} + \left(1 - \left(1-\pi\right)^k\right) \cdot p + \left(1-\pi\right)^k \cdot \rho$$

w.r.t. k to obtain the extreme value rounded up to the nearest integer, depending on π. We also give the ratio $\frac{\mathcal{T}}{\sigma}$, namely, the number of tests needed to use for one individual during the testing process. We summarize these results in Figure 6.4; the optimal pool size k which maximizes σ for a given interval of prevalence π and the corresponding value of $\frac{\mathcal{T}}{\sigma}$.

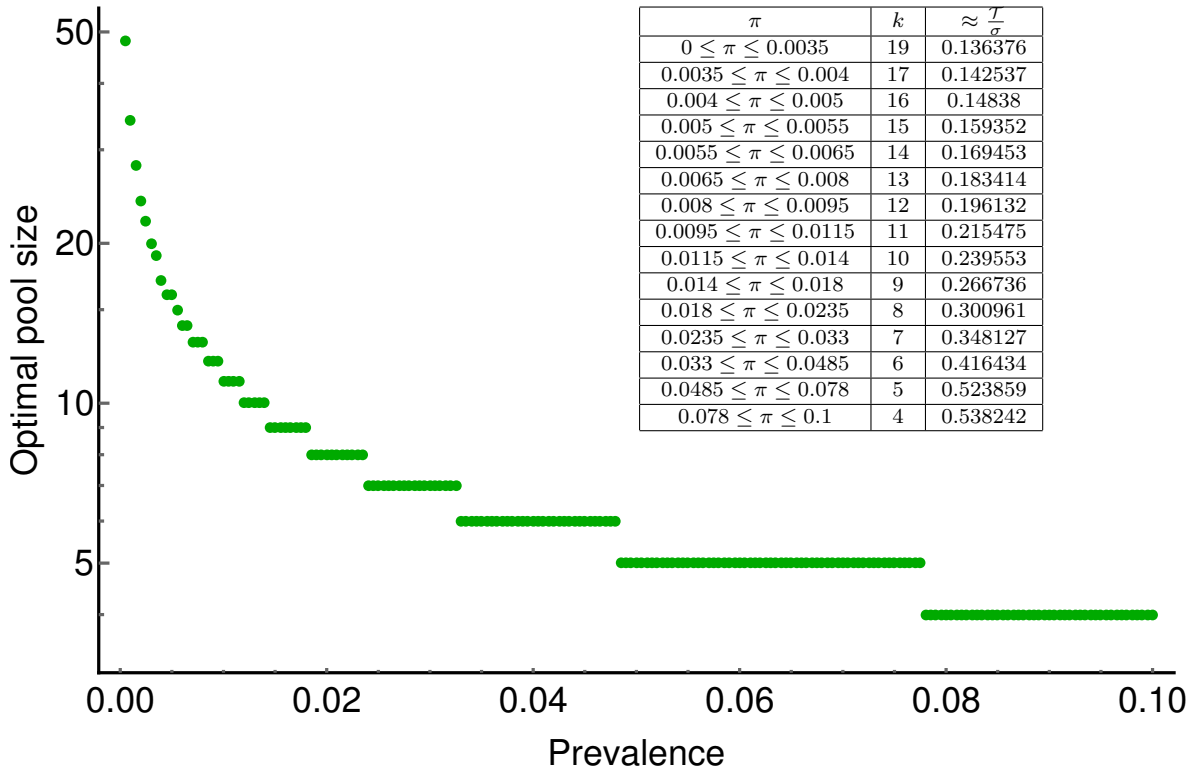

π	k	$\approx \frac{\mathcal{T}}{\sigma}$
$0 \leq \pi \leq 0.0035$	19	0.136376
$0.0035 \leq \pi \leq 0.004$	17	0.142537
$0.004 \leq \pi \leq 0.005$	16	0.14838
$0.005 \leq \pi \leq 0.0055$	15	0.159352
$0.0055 \leq \pi \leq 0.0065$	14	0.169453
$0.0065 \leq \pi \leq 0.008$	13	0.183414
$0.008 \leq \pi \leq 0.0095$	12	0.196132
$0.0095 \leq \pi \leq 0.0115$	11	0.215475
$0.0115 \leq \pi \leq 0.014$	10	0.239553
$0.014 \leq \pi \leq 0.018$	9	0.266736
$0.018 \leq \pi \leq 0.0235$	8	0.300961
$0.0235 \leq \pi \leq 0.033$	7	0.348127
$0.033 \leq \pi \leq 0.0485$	6	0.416434
$0.0485 \leq \pi \leq 0.078$	5	0.523859
$0.078 \leq \pi \leq 0.1$	4	0.538242

Figure 6.4: Optimal pool size as a function of disease prevalence.

6.5 Strategies employing optimized Dorfman pooling

In this section, we present some numerical results employing optimized strategies with Dorfman pooling.

6.5.1 Fixed pool size during the pandemic

First, we consider different, fixed pool size values k which we apply in (6.2) regardless of the prevalence, and a corresponding optimized σ according to (6.3). In the following, the daily testing capacity $\mathcal{T}$ is fixed to $100,000$ which is feasible as it is 1% of the total population Π. According to the result in Section 6.4, for the optimized strategy we take $\pi = 0.1$. Figure 6.5 shows a comparison for these scenarios for different k values. We can see that choosing pool size $k = 4$ is the best strategy, and considering $\Pi = 10,000,000$, $\approx 2\%$ of the total population can avoid the infection simply by choosing another, more appropriate pool size.

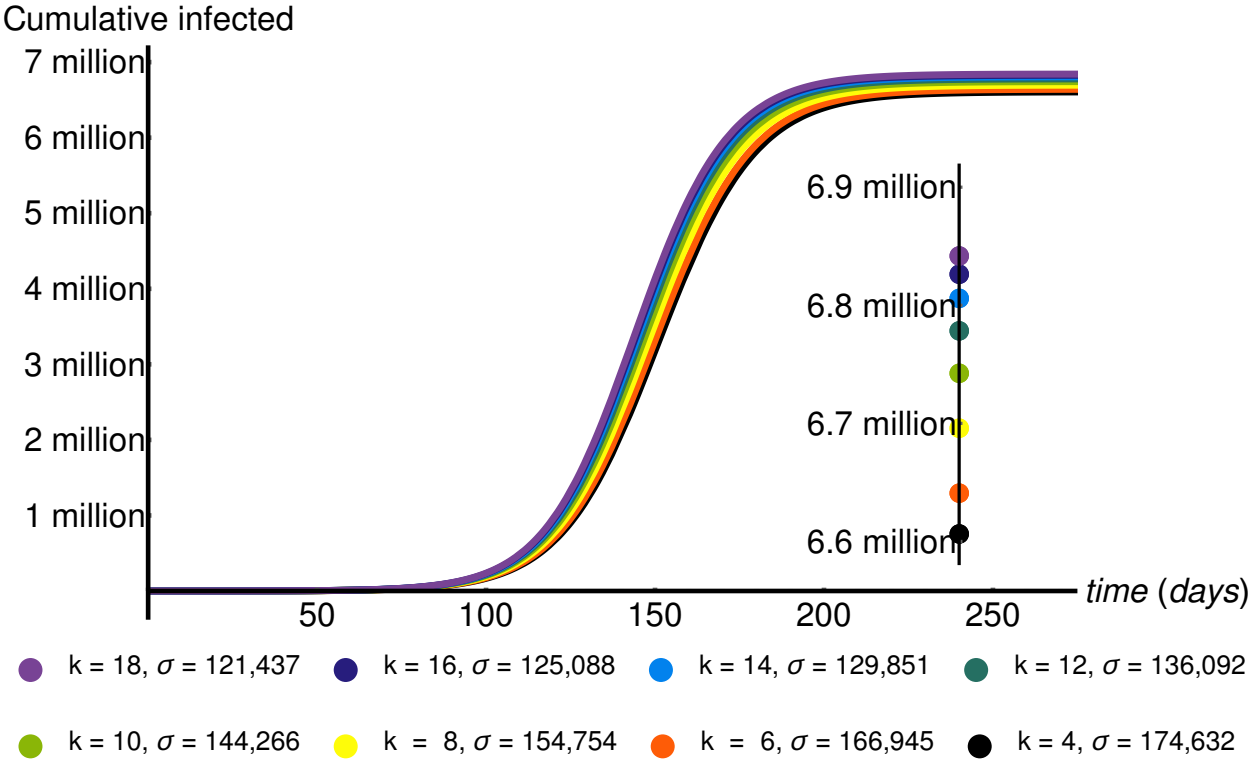

Figure 6.5: Epidemic curves of the cumulative infected with a fixed pool size during the course of the epidemic. Parameters p and ρ are taken from Table 6.1, $R_c = 1.8$.

6.5.2 Adaptive strategy: variable pool size

In this section, we consider a changing pool size $k(\pi(t))$ dependent on the disease prevalence (see Section 6.4.1). In Figure 6.6 and Figure 6.7 we compare all testing methods we discussed earlier: mass testing without pooling, regular pooling, Dorfman pooling with optimized σ

for every prevalence $0 \leq \pi(t) \leq 0.1$ and adaptive, changing pool size $k(\pi(t))$ and $\sigma(\pi(t))$. We can see that choosing a large pool size and a corresponding σ at the start of the testing allows a widespread testing opportunity in the population. This intervention is enough to prevent an outbreak (see Figure 6.6) or in the case of a bigger reproduction rate it is capable to shift the peak and flatten the curve for a foreseeable time period.

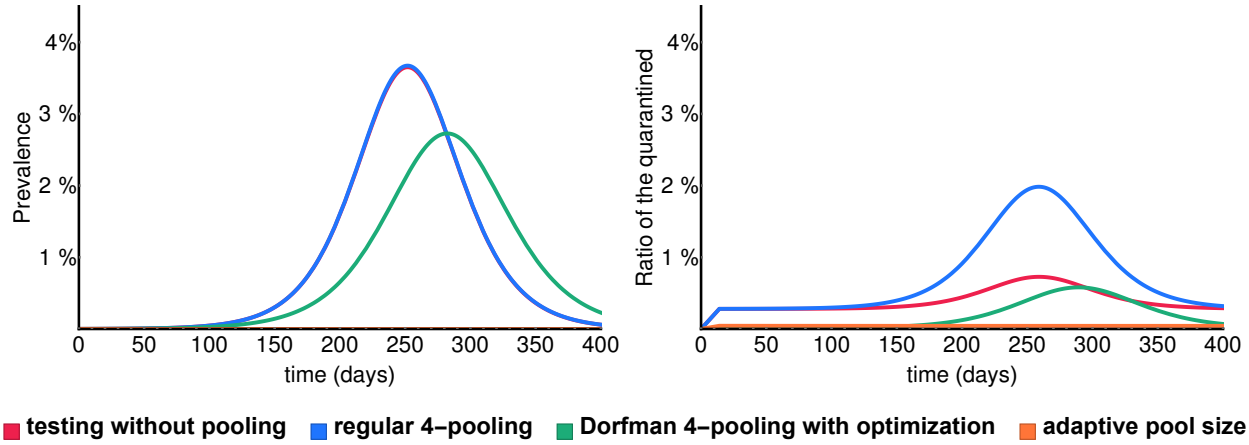

Figure 6.6: Comparison of different testing strategies. Parameters p and ρ are taken from Table 6.1, $R_c = 1.4$.

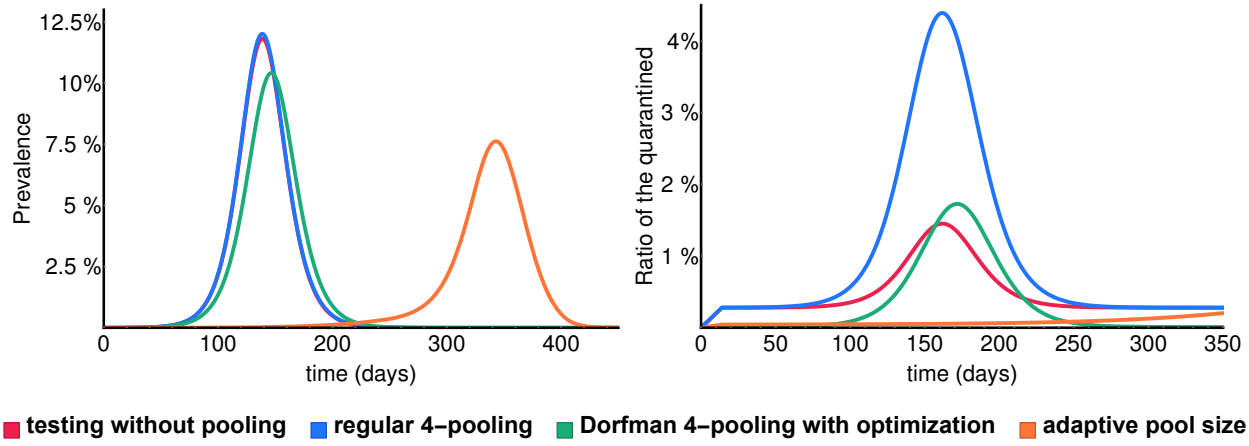

Figure 6.7: Comparison of different testing strategies. Parameters p and ρ are taken from Table 6.1, $R_c = 1.7$.

7

Summary

After a short introduction, in Chapter 2, this thesis firstly aims to give an overview on SIS models, from the very basics to extensions and generalizations.

Then, in Chapter 3 and 4, we studied a multistage SIS model, also known as $SI_1I_2 \dots I_nS$ model, where infectious individuals progress through a number of disease stages. The model was rigorously analyzed to gather information about its dynamical features. We have calculated the basic reproduction number $\mathcal{R}_0$ and shown its threshold property, namely that when $\mathcal{R}_0$ is less than or equal to 1, the disease-free equilibrium is globally asymptotically stable, and when $\mathcal{R}_0 > 1$, the disease persists uniformly in the population. So far this is a standard result for many epidemiological models. The main result of these chapters is that the stability properties of the endemic equilibrium depend on the number of infectious stages. For $n = 1, 2, 3$, the endemic equilibrium is always stable whenever exists, regardless of the particular choice of transmission and progression parameters β_j, p_j. However, for $n \geq 4$, instability of the endemic equilibrium is possible, and for any $n \geq 4$ there exist stable and unstable configurations of the parameters. In the unstable case, we expect oscillatory disease dynamics. This has an important implication for the modelling of infectious diseases with varying infectivity. During the course of infection, the infectivity of a host naturally changes continuously alongside disease progression, and this may cause oscillations, as it has been pointed out is some models in the context of HIV [34]. Multistage compartmental models represent a discretization of this variation of infectivity in time. For some cases it may very well be a possibility, that the real life disease dynamics is oscillatory, which we can capture by a model with sufficiently many stages, but an oversimplification to three or less disease stages causes that the model prediction of global stability will be false.

A somewhat similar phenomenon has been observed for waning immunity models of $SIR_1 \dots R_nS$-type, where the immune period was divided into stages, and the stability could be lost if there were at least three R-stages, see Section 4 in [24]. Since from an epidemiological point of view it does not make a difference if a host is in an R-compartment, or in an I-compartment with zero infectivity, the SIRS model in Section 4 of [24] can be considered as a very special case of our system (3.1) with $\beta_j = 0$ for $j > 1$ and $p_2 = \dots = p_n$. Similarly, multistage $SEIRS$ models can also be considered as special cases of SIS model (3.1) with setting the transmission parameter $\beta_k = 0$ for some appropriate compartments. In this regard, we found a mistake in the literature where local asymptotic stability of the endemic equilibrium in a multistage SEIRS model was claimed while in fact the endemic

equilibrium can be unstable.

Then, in Chapter 5, we have investigated the effects of indicator symptom-based testing on COVID-19. The benefits of increasing the testing rate k are demonstrated, suggesting that, as long as other logistical constraints allow, the authorities should aim to keep it as high as possible. The choice of the indicator symptom is of importance. We have shown that not just its prevalence p should be taken into account but the size and seasonality of the associated secondary symptom pool σ as well. Note that the analysis in this chapter did not directly consider contact/transmission-reducing nonpharmaceutical interventions (NPIs), *i.e.* curfew, closures of schools, wearing of masks, etc. Naturally, these interventions would affect not just the spread of COVID-19, but of other diseases, hence, potentially decreasing the secondary symptom pool σ as well. Such NPIs may be fitted into the presented framework by varying the basic reproduction number $\mathcal{R}_0$ and σ, as seen in Sect. 5.4.1.

The quality of tests was not considered. The false negativity rate could be easily modeled by a reduction factor in k. Handling the false positivity rate is more involved as susceptible individuals (susceptible to COVID-19, but still displaying the indicator symptom, *i.e.* members of σ) may be temporarily removed from the infectious chain just to reappear later, after a precautionary quarantine. However, rRT-PCR-tests have very high specificity, hence, false positives are rare.

We have modeled the transmission of COVID-19 using identical rates for the presymptomatic P and symptomatic I classes. This choice is influenced by the current understanding that according to the inferred infectivity profiles, the transmissibility prior to and after the onset of symptoms is of similar magnitude, and the ratio of presymptomatic transmissions is almost 50% [65, 66, 67]. Nevertheless, using different rates for the two compartments would not alter the computations heavily.

It is clear from the numerical simulations that indicator symptom-based testing, alone, cannot prevent an outbreak. It has a modest effect in delaying and slowing down the epidemic. Thus, symptom based testing alone may have clinical importance by providing guidance about how to treat a given patient, but its impact as epidemic mitigation is negligible. Therefore, in practice, authorities should opt to perform agile contact-tracing based on positive COVID-19 tests. The effect of this additional intervention is not included in our analysis. Nevertheless, it is safe to claim that the addition of contact-tracing would considerably increase the benefits of any testing strategy, in particular, some individuals would get removed from the presymptomatic compartment P and the latent compartment L as well via additional testing or general quarantine for contacts of COVID-19 patients with positive test result.

Then, in Chapter 6, we aim to analyse the possible application of mass testing in mitigating the epidemic. Using a system of delay differential equations, we have established a compartmental model including a temporary isolation of those tested positively (correctly or falsely) during a mass testing. We consider mass testing with pooling (i.e. mixing several samples and testing the mixed sample with a diagnostic test). We consider regular and Dorfman pooling as well. The latter means that all individuals whose sample were included in positively tested pools are tested once again, this time individually. Our results show that although it may effectively reduce the number of infected, regular pooling increases the number of quarantined people to such an extent that it makes a real-life application of this method impossible.

On the other hand, though requiring more tests, Dorfman pooling is shown to be an efficient tool. At the same time, using some kind of pooling method, we can avoid placing healthy people in quarantine unnecessarily. We have shown that choosing an optimal (fixed) pooling size, disease burden can be reduced significantly. Furthermore, if pool size is continuously adapted during the epidemic to the actual prevalence, one may achieve a remarkable reduction in the number of infections with a significant shift in the time of the epidemic peak even in the case of a severe outbreak. In the case of a milder epidemic with a lower reproduction number, applying such an intervention may even completely prevent an outbreak.

There are many layers of complexities of the COVID-19 pandemic that we have not considered in our model. Here we have focused solely on the benefits of pooling, and its optimization. As future work we propose to study the combination of pooling and more involved testing strategies, such as risk oriented testing, where risk can be assessed by symptoms, contacts, activity, or exposure.

The dissertation is based on three articles of the author. These publications are the following:

[1] G. Röst, T. Tekeli, Stability and oscillations of multistage SIS models depend on the number of stages, *App. Math. and Comp.*, (380), **2020**, 125259, 0096-3003, https://doi.org/10.1016/j.amc.2020.125259.

[2] F. A. Bartha, J. Karsai, T. Tekeli, G. Röst, Symptom-based testing in a compartmental model of COVID-19, in: P. Agarwal, J. J. Nieto, M. Ruzhansky, D. F. M. Torres (Eds.), Analysis of infectious disease problems (Covid-19) and their global impact, Springer, Singapore, 2021, pp. pp 357–376. https://doi.org/10.1007/978-981-16-2450-6_16

[3] T. Tekeli, A. Dénes, G. Röst, Adaptive group testing in a compartmental model of COVID-19. *Math. Biosci. and Eng.*, **2022**, 19(11): 11018-11033, https://doi.org/10.3934/mbe.2022513

Other publications from the author are as follows:

(i) A. Dénes, M. A. Ibrahim, L. Oluoch, M. Tekeli and T. Tekeli, Impact of weather seasonality and sexual transmission on the spread of Zika fever, Nature - Scientific Reports (9), 17055 (2019), https://doi.org/10.1038/s41598-019-53062-z

(ii) G. Röst, F. A. Bartha, N. Bogya, P. Boldog, A. Dénes, T. Ferenci, K. J. Horváth, A. Juhász, C. Nagy, T. Tekeli, Z. Vizi and B. Oroszi, Early phase of the COVID-19 outbreak in Hungary and post-lockdown scenarios, Viruses 2020, 12(7), 708, https://doi.org/10.3390/v12070708

(iii) P. Boldog, T. Tekeli, Z. Vizi, A. Dénes, F. A. Bartha and G. Röst, Risk Assessment of Novel Coronavirus COVID-19 Outbreaks Outside China, J. Clin. Med. 2020, 9(2), 571, https://doi.org/10.3390/jcm9020571

(iv) F. A. Bartha, P. Boldog, T. Tekeli, Zs. Vizi, A. Dénes and G. Röst, Potential severity, mitigation, and control of Omicron waves depending on pre-existing immunity and immune evasion, in: R. P. Mondaini (Ed.), Trends in Biomathematics: Stability and Oscillations. Springer Nature Switzerland AG, Basel. (2022), https://doi.org/10.1101/2021.12.15.21267884

8

Összefoglaló

A disszertáció célja, hogy fertőző betegségek terjedésének dinamikáját leíró matematikai modelleket állítson fel, valamint e modellek matematikai analízisét végezze el. A bevezetés után a 2. fejezetben az SIS járványterjedési modelleket tekintjük át, a legegyszerűbbtől kezdve az általánosított és továbbfejlesztett konstrukciókig. Majd, a 3. és 4. fejezetekben egy több fertőző szakaszból álló $SI_1I_2 \dots I_nS$ modellt vizsgálunk. Meghatározzuk a dinamika szempontjából legfontosabb jellemzőket, az $\mathcal{R}_0$ reprodukciós számot és annak fontos küszöbtulajdonságát, nevezetesen, ha $\mathcal{R}_0$ kisebb vagy egyenlő, mint 1, akkor a betegségmentes egyensúly globálisan aszimptotikusan stabil, ha pedig ez a mennyiség nagyobb, mint 1, akkor a betegség egyenletesen perzisztens a populációban. Ezzel analóg eredmények az irodalomban számos epidemiológiai modellel kapcsolatos munkában megtalálhatók. A 3. és 4. fejezet fő eredménye, hogy az endemikus egyensúly stabilitása nagyban függ a fertőző szakaszok számától. Ha a fertőző I osztályt $n = 1, 2$ vagy 3 szakaszra osztjuk, a paraméterek választásától függetlenül az endemikus egyensúly mindig stabil, amikor létezik. Viszont, $n \geq 4$ fertőző szakasz esetén minden n-re választhatók a paraméterek úgy, hogy az endemikus egyensúly stabil legyen, de ugyanolyan n-re létezik olyan paraméterválasztás is, hogy az endemikus egyensúly instabil legyen. Az instabil esetben oszcilláló dinamika figyelhető meg. A fejezet eredményeinek következményei igen fontosak lehetnek a váltakozó fertőzékenységű betegségek, mint például a HIV modellezésének kapcsán, ahol az oszcilláló dinamika lehetőségét a [34] cikk vizsgálja. A több fertőző szakaszból álló, ún. *multistage* modellek diszkretizálják ezt a változó fertőzékenységet. Az oszcilláló dinamikát megfelelő számú fertőző szakasz bevezetésével meg lehet jeleníteni a modellben, de egy túlságosan leegyszerűsített konstrukció tévesen feltételezett globális stabilitást eredményezhet.

Hasonló jelenség figyelhető meg az eltűnő immunitást modellező, $SIR_1R_2 \dots R_nS$-típusú modellek esetében, ahol az immunis, R-periódus van szakaszokra osztva. Ha legalább három R kompartmentre bontjuk az immunis időszakot, oszcilláló dinamika következhet be, lásd a [24] 4. fejezetét. Epidemiológiai szempontból ekvivalens, ha a személy egy nulla fertőzékenységű I-nek nevezett, vagy egy immunis, R-nek nevezett periódusban található, így a [24] cikk 4. fejezetében szereplő $SIRS$ modell a (3.1) modell egy speciális esetének tekinthető, zéró fertőzési ráták és egyenlő $p_2 = \dots = p_n$ paraméterek esetén. Hasonlóképp, a több szakaszra bontott $SEIRS$-típusú modellek a transzmissziós β_k paraméterek megfelelő választása esetén az (3.1) SIS-modell speciális esetének tekinthetők. Így, az irodalomban szereplő néhány cikkben az endemikus egyensúly általános lokális stabilitásáról szóló eredmények tévesek.

Ezután, az 5. fejezetben a COVID-19 indikátortünet-alapú tesztelésének hatásait vizsgáljuk. A k tesztelési ráta növelésének előnyeit mutatjuk be. Eredményünk szerint érdemes a lehető legmagasabb tesztelési rátát alkalmazni, amíg ezt más, pl. logisztikai szempontok lehetővé teszik. Az indikátortünet megfelelő megválasztása is nagy jelentőséggel bír, megmutatjuk, hogy ehhez nem csak a p prevalenciát kell figyelembe venni, hanem az ún. *másodlagos tünetesek* csoportjának méretét és szezonalitását. Megjegyezzük, hogy ebben a munkában nem vettünk figyelembe egyéb, nem-farmakológiai intézkedéseket (iskolák bezárása, maszkviselés, stb.). Ezen intézkedések használata nem csak a COVID-19 terjedését csökkenti, hanem más betegségekét is, így a másodlagos tünetesek csoportjának σ méretét is. A nem-farmakológiai intézkedéseket az $\mathcal{R}_0$ alap reprodukciós szám és a σ változtatásával tudjuk megjeleníteni a modellben, lásd az 5.4.1 fejezetet. A fejezetben szereplő tesztelésnél elhanyagoljuk a fals negatív és fals pozitív tesztarányt. A fejezetben a COVID-19 terjedésének kapcsán mindenhol feltesszük, hogy a tünetmentesen fertőző P és a tüneteket produkáló fertőző I osztályba tartozók ugyanolyan rátával fertőznek. Ezt a választást a [65, 66, 67] cikkek indokolták. Megjegyezzük, hogy különböző rátákat alkalmazva a P és az I osztályban, a modell dinamikája nem változik jelentős mértékben.

Szimulációink megmutatják, hogy az indikátortünet-alapú tesztelés önmagában nem alkalmas egy járványkitörés megelőzésére, pusztán a járvány csúcsának mérsékelt késleltetésére és a terjedés csillapítására. Ezért, a e módszer a járvány kezelésének szempontjából nem jelentős. Így a hatóságok számára inkább hatékony kontaktkutatás javallott, mely eljárás modellezésére a fejezet nem tér ki.

Ezután, a 6. fejezetben tömeges tesztelési eljárások modellezését mutatjuk be. Késleltetett differenciálegyenlet-rendszert használva, ún. *kompartmentális* modellt alkotunk, amelyben a pozitív tesztet adók ideiglenes izolációja is szerepel. Kétféle ún. *pooling* teszteléssel (a módszer több minta összeöntését, majd az összeöntött minta egy mintaként történő kiértékelését jelenti) is foglalkozunk, bemutatjuk e tesztelés reguláris, illetve a Dorfman-féle variációját. Utóbbi jelentése, hogy a pozitív eredményt produkáló csoportokban összeöntött mintákon külön-külön elvégzett teszteket hajtunk végre. Megmutatjuk, hogy ezzel a fertőzöttek száma bár jelentősen lecsökkenthető, a csoportos tesztelési eljárás miatt megnövekedett fals pozitív arány miatt a karanténba kerültek száma oly magas, ami a módszert alkalmazhatatlanná teszi.

Összehasonlításunk alapján, habár az egyéni tesztek száma miatt nagyobb kapacitást igénylő intézkedésről van szó, a Dorfman-féle csoportos tesztelés hatékony beavatkozásnak minősíthető. Ezzel egyidejűleg, a mintákat megfelelően csoportosítva, hatékonyabbá tehetjük az eljárást. Megmutatjuk, hogy optimalizált csoportméretet választva, jelentős számú megbetegedést és elhalálozást akadályozhatunk meg. Továbbá rámutatunk, hogy adaptív módszerrel, a prevalenciától függő, optimalizált csoportméretet használva a járvány terjedése még jobban csillapítható. A járvány csúcsa nagyobb reprodukciós szám esetén is késleltethető, kisebb $\mathcal{R}_0$ esetén pedig ez az intézkedés a járvány kitörését is megfékezheti. A fejezetben szereplő modell tovább pontosítható. A csoportos tesztelési módszer, más módszerekkel, pl. az indikátortünetek figyelembe vételével egy jövőbeli kutatás alapját képezheti.

A disszertáció a szerző három munkáján alapul, ezek a következők:

[1] G. Röst, T. Tekeli, Stability and oscillations of multistage SIS models depend on the number of stages, *App. Math. and Comp.*, (380), **2020**, 125259, 0096-3003, https://doi.org/10.1016/j.amc.2020.125259.

[2] F. A. Bartha, J. Karsai, T. Tekeli, G. Röst, Symptom-based testing in a compartmental model of COVID-19, in: P. Agarwal, J. J. Nieto, M. Ruzhansky, D. F. M. Torres (Eds.), Analysis of infectious disease problems (Covid-19) and their global impact, Springer, Singapore, 2021, pp. pp 357–376. https://doi.org/10.1007/978-981-16-2450-6_16

[3] T. Tekeli, A. Dénes, G. Röst, Adaptive group testing in a compartmental model of COVID-19. *Math. Biosci. and Eng.*, **2022**, 19(11): 11018-11033, https://doi.org/10.3934/mbe.2022513

A szerző további munkái:

(i) A. Dénes, M. A. Ibrahim, L. Oluoch, M. Tekeli and T. Tekeli, Impact of weather seasonality and sexual transmission on the spread of Zika fever, Nature - Scientific Reports (9), 17055 (2019), https://doi.org/10.1038/s41598-019-53062-z

(ii) G. Röst, F. A. Bartha, N. Bogya, P. Boldog, A. Dénes, T. Ferenci, K. J. Horváth, A. Juhász, C. Nagy, T. Tekeli, Z. Vizi and B. Oroszi, Early phase of the COVID-19 outbreak in Hungary and post-lockdown scenarios, Viruses 2020, 12(7), 708, https://doi.org/10.3390/v12070708

(iii) P. Boldog, T. Tekeli, Z. Vizi, A. Dénes, F. A. Bartha and G. Röst, Risk Assessment of Novel Coronavirus COVID-19 Outbreaks Outside China, J. Clin. Med. 2020, 9(2), 571, https://doi.org/10.3390/jcm9020571

(iv) F. A. Bartha, P. Boldog, T. Tekeli, Zs. Vizi, A. Dénes and G. Röst, Potential severity, mitigation, and control of Omicron waves depending on pre-existing immunity and immune evasion, in: R. P. Mondaini (Ed.), Trends in Biomathematics: Stability and Oscillations. Springer Nature Switzerland AG, Basel. (2022), https://doi.org/10.1101/2021.12.15.21267884

Bibliography

[1] G. Röst, T. Tekeli, Stability and oscillations of multistage SIS models depend on the number of stages, *App. Math. and Comp.*, (380), **2020**, 125259, 0096-3003, https://doi.org/10.1016/j.amc.2020.125259.

[2] F. A. Bartha, J. Karsai, T. Tekeli and G. Röst, Symptom-based testing in a compartmental model of COVID-19, in: P. Agarwal, J. J. Nieto, M. Ruzhansky, D. F. M. Torres (Eds.), Analysis of infectious disease problems (Covid-19) and their global impact, Springer, Singapore, 2021, pp. pp 357–376. https://doi.org/10.1007/978-981-16-2450-6_16

[3] T. Tekeli, A. Dénes and G. Röst, Adaptive group testing in a compartmental model of COVID-19. *Math. Biosci. and Eng.*, **2022**, 19(11): 11018-11033, https://doi.org/10.3934/mbe.2022513

[4] P. Boldog, T. Tekeli, Zs. Vizi, A. Dénes, F.A. Bartha and G. Röst, Risk Assessment of Novel Coronavirus COVID–19 Outbreaks Outside China. *J. Clin. Med.* **2020**, *9(2)*, 571. https://doi.org/10.3390/jcm9020571.

[5] Z. Feng, Applications of epidemiological models to public health policymaking: the role of heterogeneity in model predictions. World Scientific, 2014, https://doi.org/10.1142/8884

[6] T. Péni, B. Csutak, G. Szederkényi, G. Röst, Nonlinear model predictive control for COVID-19 management. *Nonlinear Dynamics*, **2020**; *102(4)*, 1965-1986, https://doi.org/10.1007/s11071-020-05980-1

[7] C. Yang, Y. Wang, A mathematical model for the novel coronavirus epidemic in Wuhan, China. *Mathematical Biosciences and Engineering,* **2020**, *17(3)*, 2708–2724. https://doi.org/10.3934/mbe.2020148.

[8] D. W. Berger,K. F. Herkenhoff, S. Mongey, An SEIR Infectious Disease Model with Testing and Conditional Quarantine. *NBER* **2020**, *Working Paper No. 26901*. https://doi.org/10.3386/w26901.

[9] J.S. Weitz, COVID-19 Epidemic Risk Assessment for Georgia. *Github* **2020.03.24.** https://github.com/jsweitz/covid-19-ga-summer-2020.

[10] G. Röst, *et al.* Early phase of the COVID-19 outbreak in Hungary and post-lockdown scenarios. *Viruses* **2020**, *12(7)*, 708. https://www.mdpi.com/1999-4915/12/7/708.

[11] E. Lofgren, N.H. Fefferman, Y.N. Naumov, J. Gorski, E.N. Naumova, Influenza Seasonality: Underlying Causes and Modeling Theories. *Journal of Virology* **2007**, *81(11)*, 5429–5436. https://doi.org/10.1128/JVI.01680-06.

[12] K.L. Olson, K.D. Mandl, Seasonal patterns of gastrointestinal illness. *Advances in Disease Surveillance* **2007**, *4*, 262. http://faculty.washington.edu/lober/www.isdsjournal.org/htdocs/articles/2188.pdf.

[13] G. Giordano,*et al.* Modelling the COVID-19 epidemic and implementation of population-wide interventions in Italy. *Nat Med* **2020**, *26*, 855–860. https://doi.org/10.1038/s41591-020-0883-7.

[14] M.V. Barbarossa, *et al.* Modeling the spread of COVID-19 in Germany: Early assessment and possible scenarios. *PLOS ONE* **2020**, *15(9)*, e0238559. https://doi.org/10.1371/journal.pone.0238559.

[15] S.A. Lauer, *et al.* The Incubation Period of Coronavirus Disease 2019 (COVID-19) From Publicly Reported Confirmed Cases: Estimation and Application. *Ann Intern Med* **2020**, *172(9)*, 577–582. https://doi.org/10.7326/M20-0504.

[16] O. Diekmann, ; J.A.P. Heesterbeek, M.G. Roberts, The construction of next-generation matrices for compartmental epidemic models. *J. R. Soc. Interface* **2020**, *7(47)*, 873–885. https://doi.org/10.1098/rsif.2009.0386.

[17] G. Chowell, P. Fenimore, M. Castillo-Garsow and C. Castillo-Chavez, SARS outbreaks in Ontario, Hong Kong and Singapore: the role of diagnosis and isolation as a control mechanism. *J. Theor. Biol.* **2003**, *224(1)*. https://doi.org/10.1098/rsif.2007.1036.

[18] A. Cori, N.M. Ferguson, C. Fraser, S. Cauchemez, A New Framework and Software to Estimate Time-Varying Reproduction Numbers During Epidemics. *Am. J. Epidemiol.* **2013**, *178(9)*, 1505–1512. https://doi.org/10.1093/aje/kwt133.

[19] J. Wallinga, M. Lipsitch. How Generation Intervals Shape the Relationship Between Growth Rates and Reproductive Numbers. *Proceedings of the Royal Society B: Biological Sciences* **2007**, *274(1609)*, 599–604. https://royalsocietypublishing.org/doi/full/10.1098/rspb.2006.3754.

[20] F. Brauer, C. Castillo-Chavez, Mathematical Models in Population Biology and Epidemiology - Second Edition, Springer (2012) ISBN: 978-1-4614-1685-2. https://doi.org/10.1007/978-1-4614-1686-9

[21] A. Dénes, Y. Muroya, G. Röst, Global stability of a multistrain SIS model with superinfection, Math. Biosci. Eng. 14:(2) (2017) 421–435, https://doi.org/10.3934/mbe.2017026

[22] O. Diekmann, J. A. P. Heesterbeek, Mathematical Epidemiology of Infectious Diseases: Model Building, Analysis and Interpretation, Wiley (2000) ISBN: 978-0-4719-8682-9, https://doi.org/10.3934/mbe.2017026

[23] H. Guo, M.Y. Li, Global dynamics of a staged progression model for infectious diseases, Math. Biosci. Eng. 3 (2006) 513-–525, https://doi.org/10.3934/mbe.2006.3.513

[24] H. W. Hethcote, H. W. Stech, P. van den Driessche, Nonlinear oscillations in epidemic models, SIAM J. Appl. Math. 40:(1) (1981) 1–9.

[25] H. W. Hethcote, H. Thieme, Stability of the Endemic Equilibrium in Epidemic Models with Subpopulations, Math. Biosci. 75 (1985) 205–227, http://dx.doi.org/10.1016/0025-5564(85)90038-0

[26] J.M. Hyman, J. Li, E.A. Stanley, The differential infectivity and staged progressing models for the transmission of HIV, Math. Biosci. 155 (1999) 77-109, https://doi.org/10.1016/s0025-5564(98)10057-3

[27] J. Li, Z. Ma, F. Zhang. Stability analysis for an epidemic model with stage structure, Nonlinear Anal. Real World Appl. 9 (2008) 1672-1679, https://doi.org/10.1016/j.nonrwa.2007.05.002

[28] J. Liu, Z. Bai, T. Zhang, A periodic two-patch SIS model with time delay and transport-related infection, J. Theor. Biol., Volume 437, (2018) 36-44, https://doi.org/10.1016/j.jtbi.2017.10.011

[29] Z. Ma, J. Liu, J. Li, Stability analysis for differential infectivity epidemic models, Nonlinear Anal. Real World Appl. 4 (2003) 841-856, https://doi.org/10.1016/S1468-1218(03)00019-1

[30] M. Marden, Geometry of Polynomials, Second Edition, Mathematical Surveys Number 3, AMS (1966), http://dx.doi.org/10.1090/surv/003

[31] D. Y. Melesse, A. B. Gumel, Global asymptotic properties of an SEIRS model with multiple infectious stages, J. Math. Anal. Appl. 366 (2010) 202–217, https://doi.org/10.1016/j.jmaa.2009.12.041

[32] Y. Nakata, G. Röst, Global stability of an SIS epidemic model with a finite infectious period, Differential and Integral Equations, 31:(3-4) (2018) 161–172.

[33] Z. Shuai, P. van den Driessche, Global stability of infectious disease models using Lyapunov functions, SIAM J. Appl. Math. 73:(4) 1513–1532, https://doi.org/10.1137/120876642

[34] H. R. Thieme, C. Castillo-Chavez, How may infection-age-dependent infectivity affect the dynamics of HIV/AIDS? , SIAM Journal on Applied Mathematics, 53(5), (1993), 1447–1479, https://doi.org/10.1137/0153068

[35] P. van den Driessche, J. Watmough, Reproduction numbers and sub-threshold endemic equilibria for compartmental models of disease transmission, Mathematical Biosciences 180:(1-2) (2002) 29–48, https://doi.org/10.1016/S0025-5564(02)00108-6

[36] P. Boldog, T. Tekeli, Z. Vizi, A. Dénes, F. A. Bartha, G. Röst, Risk assessment of novel coronavirus COVID-19 outbreaks outside China, *J. Clin. Med*, **9** (2020), 571. https://doi.org/10.3390/jcm9020571

[37] H. Nishiura, S.-M. Jung, N. M. Linton, R. Kinoshita, Y. Yang, K. Hayashi, et al., The extent of transmission of novel coronavirus in Wuhan, China, *J. Clin. Med.*, **9** (2020), 330. https://doi.org/10.3390/jcm9020330

[38] S. Jung, A. R. Akhmetzhanov, K. Hayashi, N. M. Linton, Y. Yang, B. Yuan et al., Real-time estimation of the risk of death from novel coronavirus (COVID-19) infection: inference using exported cases, *J. Clin. Med.*, **9** (2020), 523. https://doi.org/10.3390/jcm9020523

[39] World Health Organization, *Laboratory testing for coronavirus disease (COVID-19) in suspected human cases, Interim guidance*, 19 March 2020. https://www.who.int/publications-detail/laboratory-testing-for-2019-novel-coronavirus-in-suspected-human-cases-20200117

[40] Centers for Disease Control and Prevention, *Real-Time RT-PCR Panel for Detection 2019-nCoV*, 29 January 2020. https://www.fda.gov/media/134922/download

[41] P. Habibzadeh, M. Mofatteh, M. Silawi, S. Ghavami, M. A. Faghihi, Molecular diagnostic assays for COVID-19: an overview, *Crit. Rev. Clin. Lab. Sci.*, **58** (2021), 385–398. https://doi.org/10.1080/10408363.2021.1884640

[42] A. Basu, T. Zinger, K. Inglima, K. Woo, O. Atie, L. Yurasits et al., Performance of Abbott ID now COVID-19 rapid nucleic acid amplification test using nasopharyngeal swabs transported in viral transport media and dry nasal swabs in a New York City academic institution, *J. Clin. Microbiol.* **58** (2020) e01136-20. https://doi.org/10.1128/JCM.01136-20

[43] B. Berber, C. Aydin, F. Kocabas, G. Guney-Esken, K. Yilancioglu, M. Karadag-Alpaslan et al. Gene editing and RNAi approaches for COVID-19 diagnostics and therapeutics, *Gene Ther.*, **28** (2021), 290–305. https://doi.org/10.1038/s41434-020-00209-7

[44] R. W. Peeling, P. L. Olliaro, D. I. Boeras, N. Fongwen, Scaling up COVID-19 rapid antigen tests: promises and challenges, *Lancet Infect. Dis.* **21**(2021), e290–e295. https://doi.org/10.1016/S1473-3099(21)00048-7

[45] C. C. Kerr, D. Mistry, R. M. Stuart, K. Rosenfeld et al., Controlling COVID-19 via test-trace-quarantine. *Nat. Commun.*, **12**(2021), 2993. https://doi.org/10.1038/s41467-021-23276-9

[46] D. Lunz, G. Batt, J. Ruess, To quarantine, or not to quarantine: A theoretical framework for disease control via contact tracing. *Epidemics*, **34**(2021), 100428. https://doi.org/10.1016/j.epidem.2020.100428

[47] J. H. Tanne, E. Hayasaki, M. Zastrow, P. Pulla, P. Smith, A. G. Rada et al., Covid-19: how doctors and healthcare systems are tackling coronavirus worldwide, *BMJ*, **368**(2020), m1090. https://doi.org/10.1136/bmj.m1090

[48] M. Salathé, C. L. Althaus, R. Neher, S. Stringhini, E. Hodcroft, J. Fellay et al., COVID-19 epidemic in Switzerland: on the importance of testing, contact tracing and isolation, *Swiss Med Wkly.* **150**(2020), w202205. https://dx.doi.org/10.4414/smw.2020.20225

[49] R. Dorfman, The detection of defective members of large populations, *Ann. Math. Statistics*, **14**(1943), No. 4, 436–440. https://dx.doi.org/10.1214/aoms/1177731363

[50] I. Yelin, N. Aharony, E. Shaer-Tamar, A. Argoetti, E. Messer, D. Berenbaum et al., Evaluation of COVID-19 RT-qPCR test in multi-sample pools, *Clin. Infect. Dis.* **71**(2020), 2073–2078. https://dx.doi.org/10.1093/cid/ciaa531

[51] Y. Xing, G. W. K. Wong, W. Ni, X. Hu, Q. Xing, Rapid response to an outbreak in Qingdao, China, *N. Engl. J. Med.* **383** (2020), e129. https://doi.org/10.1056/NEJMc2032361

[52] Slovakia's mass coronavirus testing finds 57,500 new cases, *Financial Times*, 10 November 2020. https://www.ft.com/content/6d20007c-25ad-4d1a-b678-591acaa57df9

[53] E. Mahase, Operation Moonshot: GP clinics could be used to improve access to COVID-19 tests, *BMJ* **370**(2020), m3552. https://doi.org/10.1136/bmj.m3552

[54] Austria to roll out free home coronavirus testing from March, *The Local*, 15 February 2021. https://www.thelocal.at/20210215/free-coronavirus-home-tests-to-be-rolled-out/

[55] "Alles gurgelt", www.allesgurgelt.at.

[56] R. Verity, L. C. Okell, I. Dorigatti, P. Winskill, C. Whittaker, N. Imai, et al., Estimates of the severity of coronavirus disease 2019: a model-based analysis, *Lancet Infect. Dis.* **20** (2020), 669–677. https://doi.org/10.1016/S1473-3099(20)30243-7

[57] World Health Organization, *Considerations for quarantine of individuals in the context of containment for coronavirus disease (COVID-19), Interim guidance*, 19 March 2020. https://apps.who.int/iris/bitstream/handle/10665/331497/WHO-2019-nCoV-IHR_Quarantine-2020.2-eng.pdf

[58] J. Riou, C. L. Althaus, Pattern of early human-to-human transmission of Wuhan 2019 novel coronavirus (2019-nCoV), December 2019 to January 2020, *Euro Surveill.* **25**(2020), 2000058. https://doi.org/10.2807/1560-7917.ES.2020.25.4.2000058

[59] R. Moss, J. Wood, D. Brown, F. Shearer, A. J. Black, A. Cheng et al. Modelling the impact of COVID-19 in Australia to inform transmission reducing measures and health system preparedness *medRχiv* 2020.04.07.20056184, 2020, https://doi.org/10.1101/2020.04.07.20056184

[60] P. Kostoulas, P. Eusebi, S. Hartnack, Diagnostic Accuracy Estimates for COVID-19 Real-Time Polymerase Chain Reaction and Lateral Flow Immunoassay Tests With Bayesian Latent-Class Models, *Am J Epidemiol.* **190** 2021 (8) : 1689-1695. https://doi.org/10.1093/aje/kwab093

[61] S. Clifford, B. J. Quilty, T. W. Russell, Y. Liu, Y-W. D. Chan, C. A. B. Pearson et al., Strategies to reduce the risk of SARS-CoV-2 re-introduction from international travellers: modelling estimations for the United Kingdom, July 2020. *Euro Surveill.* **26**(2021), 2001440. https://doi.org/10.2807/1560-7917.ES.2021.26.39.2001440

[62] J. Hellewell, T. W. Russell, The SAFER Investigators and Field Study Team. et al., Estimating the effectiveness of routine asymptomatic PCR testing at different frequencies for the detection of SARS-CoV-2 infections. *BMC Med.* **19**(2021), 106. https://doi.org/10.1186/s12916-021-01982-x

[63] M. Mancastroppa, R. Burioni, V. Colizza, A. Vezzani, Active and inactive quarantine in epidemic spreading on adaptive activity-driven networks. *Phys. Rev. E* **102** 2020, 020301(R). https://doi.org/10.1103/PhysRevE.102.020301

[64] E. Csóka, Application-oriented mathematical algorithms for group testing, arXiv preprint arXiv:2005.02388, 2020. https://doi.org/10.48550/arXiv.2005.02388

[65] He, X. *et al.* Temporal dynamics in viral shedding and transmissibility of COVID-19. *Nat Med* **2020**, *26*, 672–675. https://doi.org/10.1038/s41591-020-0869-5.

[66] Ashcroft, P.; Huisman, J.S.; Lehtinen, S.; Bouman, J.A.; Althaus, C.L.; Regoes, R.R.; Bonhoeffer, S. COVID-19 infectivity profile correction. *Swiss Med Wkly* **2020**, 150:w20336 https://doi.org/10.4414/smw.2020.20336.

[67] He, X. *et al.* Temporal dynamics in viral shedding and transmissibility of COVID-19. *Nat Med* **2020**, *26*, 1491–1493. https://doi.org/10.1038/s41591-020-1016-z

List of Figures

List of Tables